Thermoelectrics

DOI: 10.1002/anie.200900598

New and Old Concepts in Thermoelectric Materials

*Joseph R. Sootsman, Duck Young Chung, and Mercouri G. Kanatzidis**

Keywords:
energy conversion · materials science · semiconductors · solid-state chemistry · thermoelectric materials

Dedicated to Professor Martin Jansen on the occasion of his 65th birthday

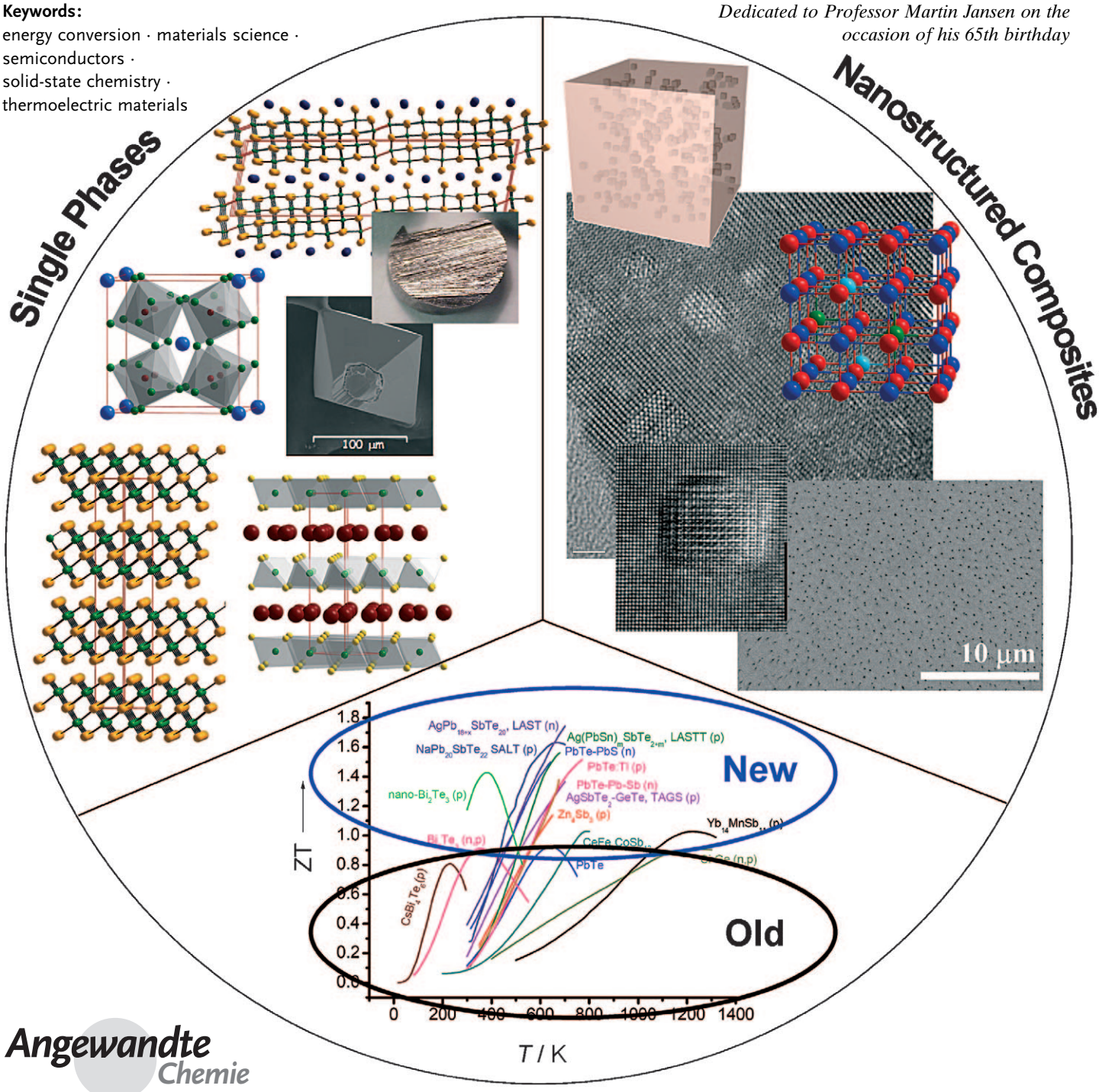

Herein we cover the key concepts in the field of thermoelectric materials research, present the current understanding, and show the latest developments. Current research is aimed at increasing the thermoelectric figure of merit (ZT) by maximizing the power factor and/or minimizing the thermal conductivity. Attempts at maximizing the power factor include the development of new materials, optimization of existing materials by doping, and the exploration of nanoscale materials. The minimization of the thermal conductivity can come through solid-solution alloying, use of materials with intrinsically low thermal conductivity, and nanostructuring. Herein we describe the most promising bulk materials with emphasis on results from the last decade. Single-phase bulk materials are discussed in terms of chemistry, crystal structure, physical properties, and optimization of thermoelectric performance. The new opportunities for enhanced performance bulk nanostructured composite materials are examined and a look into the not so distant future is attempted.

From the Contents

1. Introduction

The emerging global need for energy production, conservation, and management has intensified interest in more effective means of power generation. Enhancements to the existing energy supply must come from a variety of renewable sources including solar, wind, biomass, and others. Another potential source of power is electricity from heat sources through the use of thermoelectric materials. The heat can come from the combustion of fossil fuels, from sunlight, or as a byproduct of various processes (e.g. combustion, chemical reactions, nuclear decay). Therefore, thermoelectric materials can play a role in both primary power generation and energy conservation (i.e. waste-heat harvesting). A hot topic of discussion is how big this role is likely to be and the answer to this question depends solely on how efficient these materials are.[1] By no means should it be expected that thermoelectric energy conversion will solve the world's energy problems. It is hoped and expected however that it will play a more increasing role than it has in the past and will be one of several technologies working together to address energy efficiency issues. Thermoelectric modules are solid-state devices that directly convert thermal energy into electrical energy. This process is based on the "Seebeck effect", which is the appearance of an electrical voltage cause by a temperature gradient across a material. The inverse of this, that is, the appearance of a temperature gradient upon the application of voltage is known as the "Peltier effect".

Thermoelectric (TE) device performance relies directly on the temperature gradient (ΔT) and an intrinsic material parameter, the thermoelectric figure of merit (ZT). For power generation, the thermoelectric efficiency is defined by combining the Carnot efficiency ($\Delta T/T_{hot}$) and the figure of merit ZT as shown in Equation (1),

$$\eta = \frac{\Delta T}{T_{hot}} \frac{\sqrt{1+ZT_{avg}}-1}{\sqrt{1+ZT_{avg}}+\frac{T_{cold}}{T_{hot}}} \quad (1)$$

where T_{hot} and T_{cold} are the temperature of the hot and cold ends in a thermoelectric module and ΔT their difference. The term $(1+ZT_{avg})^{1/2}$ varies with the average temperature T_{avg}. This equation indicates that increasing efficiency requires both high ZT values and a large temperature gradient across the thermoelectric materials. Thermoelectric devices currently available have a ZT of 0.8 and operate at an efficiency of only around 5–6%. By increasing ZT a factor of 4, and depending on ΔT, the predicted efficiency increases to 30%, a highly attractive prospect.

The challenge to create high ZT thermoelectric materials lies in achieving simultaneously high electronic conductivity (σ), high thermoelectric power (S) and low thermal conductivity (κ) in the same solid.[2–11] These properties define the dimensionless thermoelectric figure of merit $ZT = (S^2\sigma/\kappa)T$ where T is the temperature. These parameters are determined by the details of the electronic structure and scattering of charge carriers (electrons or holes), and thus are not independently controllable. The quantity $S^2\sigma$ is called the power factor (PF) and is the key to achieving high performance. A large PF means that a large voltage and a high current are generated. The thermal conductivity κ has a contribution from lattice vibrations, κ_{latt}, called the lattice thermal conductivity. Thus, $\kappa = \kappa_{el} + \kappa_{latt}$, where κ_{el} is the carrier thermal conductivity. Intuitively, the thermal conductivity must be low as a large ΔT must be maintained; a large thermal conductivity will short the thermal circuit.

It is possible to envision two approaches aimed at increasing ZT: either the power factor is maximized and/or the thermal conductivity is minimized. Attempts at maximizing the power factor include the development of new classes of materials, optimization of existing materials

[*] J. R. Sootsman, Prof. M. G. Kanatzidis
Department of Chemistry, Northwestern University
2145 Sheridan Rd., Evanston, IL 60208 (USA)
E-mail: m-kanatzidis@northwestern.edu
Dr. D. Y. Chung, Prof. M. G. Kanatzidis
Materials Science Division, Argonne National Lab
Argonne, IL 60439 (USA)

through doping, and the exploration of nanoscale materials. The minimization of thermal conductivity can come through solid-solution alloying, the development of materials with intrinsically low thermal conductivity, and the relatively recent realization that significantly reduced thermal conductivity can be achieved through nanostructuring. Each of these approaches and developments will be described in the following sections.

The field of thermoelectrics presents an important challenge to synthetic chemists, physicists, as well as materials scientists. The discovery of new promising materials requires a combination of theoretical guidance, keen chemical intuition, synthetic chemistry expertise, materials processing, and good measurement skills. This powerful combination can be effectively achieved by reaching across scientific disciplines.

The purpose of this Review is to highlight some of the most promising thermoelectric materials and research results to date. It is not intended to be an exhaustive review, for example, although thin-film superlattices and nanowires are a significant part of thermoelectric research, they are not the focus of this Review. These systems have been reviewed extensively previously.[12–15] Also, it is not our intent to cover every report of measurements of thermoelectric properties if those compounds do not appear to be promising at this time. Instead, the weight of this Review lies in describing the most promising bulk materials with particular emphasis on results from the last decade.

2. Searching for the Best Thermoelectric Materials

2.1. Reducing Thermal Conductivity

Despite the linear dependence of the power factor (PF) on electrical conductivity it is not always advantageous to have a very high conductivity because this increases the electronic contribution of κ according to the Wiedeman–Franz (WF) law ($\kappa_{el} = L\,\sigma T$, where L is the Lorenz number). Typically the Lorenz number is taken to be $2.45 \times 10^{-8}\,W\Omega\,K^{-2}$ for metals and degenerate semiconductors, however it can vary depending on temperature and material.[16] Based on the WF law the electrical conductivity scales linearly with the carrier thermal conductivity κ_{el} and thus very high electronic conductivities (> 2000–$3000\,S\,cm^{-1}$ at room temperature) may not be appropriate. For the purposes of illustration, let us consider the total thermal conductivity of the best thermoelectrics used for power-generation applications, for example, for n-type PbTe the total thermal conductivity is $1.3\,W\,m^{-1}\,K^{-1}$ at 700 K. For optimized samples, about $0.15\,W\,m^{-1}\,K^{-1}$ of this value is due to κ_{el} which arises from an electronic conductivity of approximately $200\,S\,cm^{-1}$ at 700 K. Therefore, for every $200\,S\,cm^{-1}$ increase in conductivity, the thermal conductivity is burdened with an additional $0.15\,W\,m^{-1}\,K^{-1}$ (at 700 K). This places severe constraints on the magnitude of the lattice thermal conductivity to achieve high ZT.

An effective way to maximize the figure of merit (ZT) is to manipulate the lattice thermal conductivity, which is the only parameter not determined by the electronic structure. All other material parameters, such as electrical conductivity and thermoelectric power, are correlated with the electronic structure of the material and thus, in most cases, cannot be optimized independently.

The classical kinetic theory provides a good approximation for the lattice thermal conductivity [Eq. (2)]

$$\kappa_{latt} = {}^1\!/_3 C_v l v_s \tag{2}$$

where C_v is the specific heat at constant volume, l is mean free phonon path, and v_s is the average velocity of sound.[17] At very low temperatures (under 40 K), the behavior of κ_{latt} is dominated by the Debye T^3 law for C_v. Phonon scattering is insignificant in this temperature range, because of the low number of excited phonons and their very long wavelength. However, at high temperatures, that is, above the Debye temperature, C_v approaches the classical value of $3R$, making κ_{latt} primarily depend on l which is determined by phonon–phonon scattering. According to the Keyes' expression[18] the lattice thermal conductivity is dominated primarily by phonon–phonon scattering [Eq. (3)]

$$\kappa_{latt} T = \frac{R^{3/2}}{3\gamma^2 \varepsilon^3 N_0^{1/3}} \frac{T_m^{3/2} \rho^{2/3}}{A^{7/6}} \tag{3}$$

where T_m is the melting point, A is the mean atomic weight, γ is the Grüneisen constant, ε is the fractional amplitude of

Mercouri Kanatzidis holds a BSc from Aristotle University in Thessaloniki (Greece), and a PhD in chemistry from the University of Iowa. He was a post-doctoral research associate at the University of Michigan and Northwestern University from 1985 to 1987. At Northwestern University he is currently the Charles E. and Emma H. Morrison Professor of Chemistry and holds a joint appointment at Argonne National Lab, Materials Science Division. His research interests include synthesis from chalcogenide to intermetallic compounds, thermoelectric materials, and porous semiconductors.

Duck Young Chung has a B.S. in chemistry from Dankook University, Korea, and obtained his PhD by 1991 from Kyungpook National University. He then joined the group of Prof. Mercouri Kanatzidis as a postdoc at Michigan State University where he worked in the area of inorganic chemistry and materials science until 2006. His interests are synthesis, crystal growth, and characterization of solid-state chalcogenides, intermetallic alloys, and transition metal coordination compounds as well as development of material synthesis methods. He is currently a staff scientist at Materials Science Division, Argonne National Laboratory where he is involved in the development of high-temperature thermoelectric materials and new classes of superconductors.

interatomic thermal vibration, R is the ideal gas constant, N_o is Avogadro's number, and ρ is the density. This equation allows some useful insight into thermal conductivity: 1) in the high temperature range κ_{latt} follows a $1/T$ law, 2) a low melting point can lead to a low thermal conductivity, 3) κ_{latt} decreases with increasing atomic mass, and 4) the proportionality to $\rho^{2/3}$ makes κ_{latt} low for crystals with large interatomic distances.

Historically, a successful strategy to increase the ZT value has been to modify an already promising compound by introducing point defects through the synthesis of isostructural solid solutions. The solid solutions provide an environment of atomic mass fluctuation throughout the crystal lattice (i.e. disorder) which induces strong phonon scattering and generally can lead to significantly lower thermal conductivity and a larger ZT value. The canonical example of this is the Bi_2Te_3 system for which the $Bi_{2-x}Sb_xTe_3$, $Bi_2Te_{3-x}Se_x$ solid solutions are superior to the parent compound. The benefit results mainly from a lower thermal conductivity ($1.5\ W\,m^{-1}\,K^{-1}$ versus $2.4\ W\,m^{-1}\,K^{-1}$ in the parent compound) and leads to a room temperature $ZT \approx 1$ (compared with $ZT \approx 0.6$ for the parent Bi_2Te_3.

An intriguing idea to achieve maximum ZT was proposed by Slack and is referred as the "phonon glass electron crystal" (PGEC) approach.[19] A PGEC material features cages or tunnels in its crystal structure inside which reside massive atoms that are small enough relative to the cage to "rattle". This situation produces a phonon damping effect that can result in dramatic reduction of the lattice thermal conductivity. In the PGEC picture a glass-like thermal conductivity can in principle coexist with charge carriers of high mobility. An indication for a "rattling" atom is a highly elevated thermal atomic displacement parameter,[20,21] although this phenomenon by itself is not adequate as proof of PGEC. The PGEC approach has stimulated a significant amount of new research and has led to significant increases in ZT for several compounds such as the clathrates (see Section 3.1.2).

The thermal conductivity can also be decreased by increasing the lattice period (i.e. large unit cell parameters) thus providing short mean path lengths (by providing a longer more "tortuous" path through the unit cell) for the heat carrying phonons. This effect was observed in ternary and quaternary bismuth chalcogenides which form complex structures with large unit cells.

Joseph Sootsman received his bachelor's degree in chemistry from the University of Michigan in 2004 and then joined the group of Prof. Mercouri Kanatzidis at Michigan State University. He then moved to Northwestern University where he earned a PhD. He is interested in the synthesis and characterization of nanostructured and complex composite thermoelectric materials. He is currently a materials scientist at ZTPlus.

Additional highly successful strategies utilize boundary scattering as a route for reducing the lattice thermal conductivity to impressively low levels.[22,23] One such approach is grinding a material and subsequently pressing it into a pellet using hot pressing or spark plasma sintering techniques. In several cases the effect on phonon scattering was shown to be stronger than the effect on electron scattering. Another approach is to grow superlattices with a nanostructured phase within a matrix material. Finally, major reductions in the thermal conductivity have come through nanostructuring bulk materials through top down approaches. Several synthetic techniques have been applied to prepare nanostructured PbTe, for example, with exceptional reductions in the thermal conductivity. Specific examples involving these techniques for reducing thermal conductivity are presented in Section 3.3.

2.2. Increasing the Power Factor

The least understood problems in current research are how to increase the thermoelectric power of a material without depressing the electrical conductivity and to predict precisely which materials will have a high power factor. Generally, the thermoelectric power and electrical conductivity change in opposite directions with doping and thus there is a compromised set of values that must be achieved. Thus, in semiconductors there is a certain optimum carrier concentration. This behavior is normal and well understood with standard charge-transport theory. However there have been examples of a substantial increase of one quantity while the other remains constant, or a simultaneous increase of both quantities. Such effects occurred in doped polycrystalline $Ca_3Co_2O_6$ as a result of increased carrier density, mobility, and improved microstructure,[24] in ErAs/InGaAs[25] through electron filtering,[26] in nanostructured PbTe with Pb and Sb[27] through a modified carrier-scattering mechanism, in sodium-doped V_2O_5 thin film through a lowered activation energy of small polaron hoping,[28] in gold-doped Ge-Sb film through increased grain size and carrier concentration,[29] and in mixed oxides In_2O_3-SnO_2 and In_2O_3-ZnO through hoping conduction of electron and large carrier mobility.[30] These results raise hope that substantial progress can be made if these effects are better understood and controlled.

Currently, bulk materials with exceedingly large power factors in the temperatures of interest (e.g. 300–1200 K) remain elusive partly because we do not really know how a large electrical conductivity and thermoelectric power can coexist in a single compound. The development of charge-transport theory addressing how the conventional interdependence of the electrical conductivity and thermoelectric power can be bypassed is in its infancy.

As mentioned above the greatest challenge now is how to increase the thermopower of a material without depressing the electronic conductivity. Moreover, it is not clear whether this can be achieved with the already known materials or if it would require completely new systems. The details of the electronic structure are intimately tied to this question. There are two formulae that capture some of the essential physical

parameters relevant to the power factor which give a small degree of guidance, albeit generic.

Boltzmann transport theory describes both electronic and thermal transport in the vast majority of solids. This theory provides a general understanding of the thermopower that is expressed in the Mott equation [Eq. (4)][31] and the maximum

$$S = \frac{\pi^2}{3}\frac{k^2 T}{e}\frac{\mathrm{d}\ln\sigma(E)}{\mathrm{d}E}\bigg|_{E=E_f} \quad (4)$$

attainable figure of merit (Z_{max}) of Equation (5).

$$Z_{max} \propto \gamma \frac{T^{3/2}\tau_z\sqrt{\frac{m_x m_y}{m_z}}}{\kappa_{latt}} e^{(r+1/2)} \quad (5)$$

$\sigma(E)$ is the electronic conductivity determined as a function of the band filling or Fermi energy, E_F. If electronic scattering is independent of energy, then $\sigma(E)$ is just proportional to the density of states (DOS) at E. Figure 1 shows two hypothetical

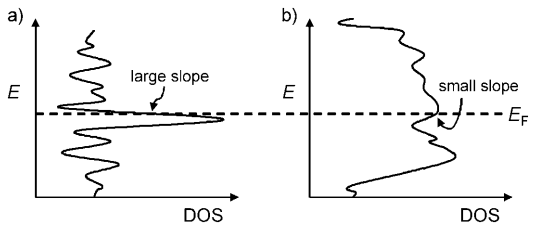

Figure 1. Hypothetical density of state (DOS) with a) a large slope ($\mathrm{d}\ln\sigma(E)/\mathrm{d}E$) and b) a small slope near E_f.

electronic DOS diagrams. One in which the DOS varies rapidly near E_F, and one in which it does not. Based on Equation (4), the system in Figure 1a with rapidly changing DOS is expected to have a larger thermoelectric power.

Another very useful expression is Equation (5) where γ is the degeneracy of band extrema, m_i is the effective mass of the carriers (electrons or holes) in the i-th direction, τ_z is the relaxation time of the carriers moving along the transport (z) direction, r is the scattering parameter, and κ_{latt} is the lattice contribution to the thermal conductivity.

What insights can be gleaned from these equations that would guide the synthetic chemist and materials scientist design or improve a thermoelectric material? In the general case, the S in the Mott equation is a measure of the variation in $\sigma(E)$ above and below the Fermi surface, specifically through the logarithmic derivative of σ with E. The thermopower of a material is a measure of the asymmetry in electronic structure and scattering rates near the Fermi level. Thus the aim should be to produce complexities in either or both the electronic structure and scattering rates within a small energy interval (a few kT) near E_F. The Mott equation does not imply anything about the magnitude of the electrical conductivity. Intuitively we could expect compounds with complex structures and compositions to have a good chance of possessing complex electronic structures. In addition, we expect composite materials, especially those with nanoscale features to produce emergent electronic structures with considerable complexity.

Examples of two semiconductors, one with a simple and one with a complex electronic structure are shown schematically in Figure 2. The band structure in Figure 2a is simple

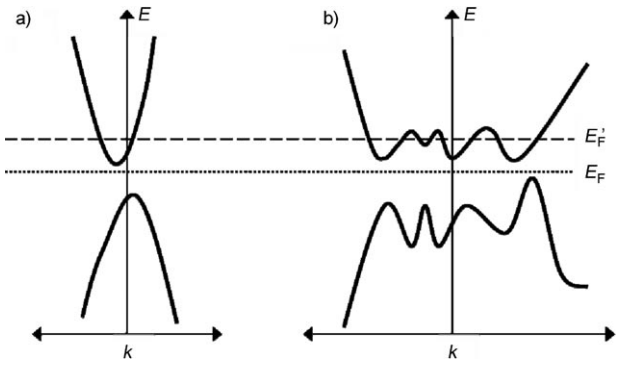

Figure 2. Hypothetical electronic band structure with a) single extremum and b) multiple extrema in the valence and conduction bands. When these systems are n-doped (see E_f' level), more extrema (electron "pockets") are populated in system (b) than in system (a). The power factor depends upon the number of populated extrema and therefore system (b) will have a higher power factor.

with only one band extremum in the valence band and one in the conduction band, while that in Figure 2b is complex with multiple extrema in both the valence and conduction bands. Simply, it can be expected that the complex structure produces a large power factor than the simple one of similar carrier concentration (p-type or n-type).

The Z_{max} of Equation (5) is insightful and has several materials implications. The degeneracy of band extrema (γ) is the number of valleys in the conduction band (relevant to n-type materials) or peaks in the valence band (relevant to p-type materials) and according to Equation (5) it needs to be high. This assumption is reasonable because each band extremum, if occupied by carriers, contributes a certain thermopower and electrical conductivity (i.e. a certain power factor).[32] The presence of a large number of such valleys in the band structure could lead to increased ZT because the total power factor for the material derives from the summation of contributions from all extrema.[33,34] Implicit in all of this is that only one type of carrier must be present in the system (electrons or holes). Mixed carrier systems have low Seebeck coefficients because of cancellation of thermal currents, ($S = S_n + S_p$). Finally, for high band degeneracy high crystal symmetry of the materials is implied (e.g. hexagonal, tetragonal, or cubic). A detailed analysis of the electronic structure of a semiconducting compound (obtained through appropriate quantum mechanical calculations) can give information about the gap, the degeneracy of the conduction and valence band extrema (i.e. γ), and even the effective mass parameters.

The Z_{max} expression in Equation (5) also involves the ratio of effective masses with respect to carrier flow. If transport is along the z-direction, the equation implies that a small

effective mass (m_z) coupled with very large masses along the x and y directions (m_x and m_y) should lead to a high ZT. For a high ($m_x m_y/m_z$) ratio a high anisotropy in the electronic structure could be expected, implying high anisotropy in the crystal structure. This implication seems contradictory to the above suggestion of the benefits of high crystal symmetry and herein lies part of the challenge in this research. There are multiple ways to approach the problem as both isotropic and anisotropic materials can be of interest. Therefore, different, possibly divergent, strategies are required to discover high-ZT systems.

From the above discussion, important parameters to consider when selecting or designing material systems are the band-gap size, the shape and width of the bands near the Fermi level (E_F), and the carrier effective masses and mobilities. The band gap is important because, in general, the temperature at which the ZT maximizes scales with band-gap size. This is because for a given band gap energy (E_g) there is a temperature at which thermally induced cross-gap carrier excitations occur to generate carriers of opposite sign which decrease the thermopower. It has been shown that semiconductors with a band gap of approximately $10\,k_B\,T$ best satisfy this criterion.[35] Thus, for cooling applications lower band-gap materials are best whereas for high-temperature power generation larger gaps are necessary. Qualitatively, the higher the E_g the higher the temperature at which the maximum in ZT will be reached before it declines.

The transport theory associated with Equation (4) and Equation (5) was developed for homogeneous single-phase compounds; however, they probably apply to nanocomposites as well. Corresponding theory for inhomogeneous materials is still developing. Bulk nanocomposites have emerged recently and offer additional physical effects that promise to overcome some of the aforementioned challenges. Already, some inhomogeneous systems have led to important breakthroughs in ZT as will be described in Section 3.3.

3. Materials Research and Solid-State Chemistry

Numerous thermoelectric materials systems have been developed and reviewed previously.[3,36–39] Our goal herein is to give an overview and most recent progress in thermoelectric materials. First, single-phase bulk materials will be discussed with particular attention to the chemistry, crystal structure, physical properties, and optimization of thermoelectric performance. These systems will be described in sequence based on materials class. Second, bulk nanostructured composite materials will be examined. The opportunities for enhanced performance in nanostructured materials will be discussed as well as our current understanding of this class of materials.

3.1. Single-Phase Materials

3.1.1. Skutterudites

Skutterudites are a highly promising and deeply researched class of compounds. They crystallize in the $CoAs_3$-type structure with the cubic space group $Im\bar{3}$. The structure is composed of eight corner-shared XY_6 (X = Co, Rh, Ir; Y = P, As, Sb) octahedra. In fact, the $CoAs_3$-structure type is a severely distorted version of the perovskite AB_3 type structure. Figure 3a and b show that the linked octahedra

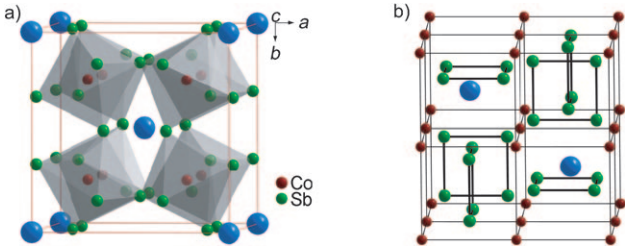

Figure 3. Two model structures of the skutterudite, $CoSb_3$; the void cages are filled with blue spheres for clarity. a) The unit cell of skutterudite structure. The transition metals (Co) are at the center of octahedra formed by pnicogen atoms (Sb). b) The model shifted by the fractional coordinates $^1/_4$, $^1/_4$, $^1/_4$ from the unit cell. The Co atoms are connected for clarity. The only chemical bonds in this model are those of the Sb squares.

produce a void at the center of the $(XY_6)_8$ cluster, where the void space occupies a body-centered position of the cubic lattice. This void is large enough to accommodate large metal atoms to form filled skutterudites. A notable characteristic of this structure is the square anionic rings of the pnicogen atoms (e.g. $[P_4]^{4-}$, $[As_4]^{4-}$, etc) which link the transition-metal ions to form the cubic structure. Therefore, the composition can be written as $\square_2X_8Y_{24}$ as illustrated in Figure 3a or $\square_2X_2[Y_4]_6$ as illustrated in Figure 3b. Jeitschko and co-workers[40–43] did some of the pioneering work on the synthesis of filled Skutterudites.

ZT values approaching 1.4 at 1000 K from 0.3 at 300 K have been predicted by a simple semiconductor transport model[44] which has helped motivate much of the work in this system. The original thermoelectric skutterudite $CoSb_3$ has a very high power factor but its lattice thermal conductivity (ca. $10\,W\,m^{-1}\,K^{-1}$ at room temperature) is too high to result in a good thermoelectric material. One successful chemical approach for optimizing these materials turned out to be void-filling in the structure with many different elements including lanthanide, actinide, alkaline-earth, alkali, thallium, and Group IV elements.[45–47] Skutterudite antimonides possess the largest voids and are thus of particular interest for thermoelectric applications.

Since the void-filling atoms can act as electron donors or acceptors, partially filling the void space of skutterudites could lead to an optimum electron concentration. At the same time, these atoms can also act as strong phonon-scattering centers to greatly reduce the lattice thermal conductivity. The "rattling" effect of these void-filling atoms has resulted in improvements in the thermoelectric properties of skutterudites.[45,47] The smaller and heavier the ion in the voids, the larger the disorder that is produced and, therefore, the larger the reduction in the lattice thermal conductivity. Although the hypothesis for the thermal conductivity reducing effect of the void-filling atoms has been based on the "rattling" property

according to the PGEC concept, "rattling" induced phonon scattering in filled skutterudites has not been proven. This is currently the subject of debate since there are additional factors, such as lattice disorder and point defects, which cannot be decoupled from any "rattling" effects. Results from Sales et al.,[44,46,48] Nolas et al.,[49] and Tang et al.[50] reported high ZT values at elevated temperatures in $La_{0.9}Fe_3CoSb_{12}$, $Ce_{0.9}Fe_3CoSb_{12}$, $Yb_xCo_4Sb_{12}$, and $Ce_yFe_xCo_{4-x}Sb_{12}$ for both p- and n-type species (Figure 4).

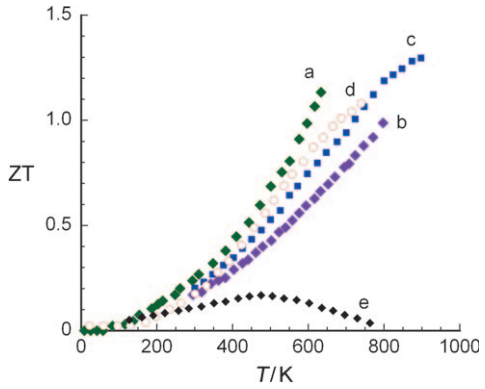

Figure 4. Figure of merit (ZT) as a function of temperature for skutterudites as thermoelectric materials: a) $Yb_{0.19}Co_4Sb_{12}$, b) $Ca_{0.18}Ni_{0.03}Co_{3.97}Sb_{12.4}$, c) $Ba_{0.30}Ni_{0.05}Co_{3.95}Sb_{12}$, and d) $Ce_{0.9}Fe_3CoSb_{12}$. The ZT of e) Co_4Sb_{12} is shown for comparison.

Interestingly, only a small concentration of La or Ce[51] in the voids of $CoSb_3$ results in a significant thermal conductivity reduction, and in some cases, have shown high power factors.[49,52] One example ($Yb_{0.19}Co_4Sb_{12}$, $ZT \approx 1$ at 600 K)[10,49] in Figure 4 shows how partial filling can result in higher ZT values than full filling. Recently, higher ZT values of partially filled skutterudites with a small amount of Ni doping for Co, $Ba_{0.30}Ni_{0.05}Co_{3.95}Sb_{12}$ ($ZT \approx 1.25$ at 900 K)[53] and $Ca_{0.18}Ni_{0.03}Co_{3.97}Sb_{12.4}$ ($ZT \approx 1$ at 800 K)[54] were reported, compared with those of $Ba_xCo_4Sb_{12}$[55] ($ZT \approx 0.8$ at 800 K) and $Ca_xCo_4Sb_{12}$[47,56] ($ZT \approx 0.45$ at 800 K).

Research into skutterudite compounds has led to further understanding of thermal-transport processes and phonon-scattering mechanisms, resulting in new efforts to seek other materials with similar properties. Although it is still an open question whether the various partially filled skutterudite derivatives are in fact PGEC materials, the conceptual appeal of Slack and Tsoukala's[57] "rattling" atom approach to skutterudite thermoelectric research has produced ZT values over 1.

3.1.2. *Clathrates*

The clathrates are generally low-thermal conductivity compounds with open frameworks composed of tetrahedrally coordinate Al, Ga, Si, Ge, or Sn. The framework has cages that can incorporate large electropositive atoms. There are two main types of structure the so-called Type I and Type II with the former being more common. The Type I structure can be represented by the general formula $X_2Y_6E_{46}$ (Figure 5a, Na_8Si_{46} for example), where X and Y are "guest" atoms encapsulated in two different polyhedral cages E_{20} and E_{24}, while E represents tetrahedrally coordinate framework atoms. The Type II structure is composed of E_{20} and E_{28} cages.

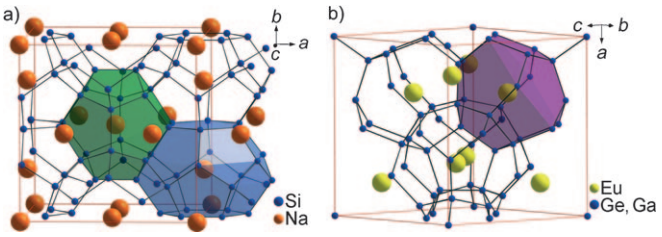

Figure 5. a) Crystal structure of the Type I clathrate, Na_8Si_{46}. Framework composed of Si atoms (blue) and two different cages with guest Na atoms, the tetrakaidecahedral cage ($[5^{12}6^2]$; blue) and the pentagonal dodecahedral cage ($[5^{12}]$; green). b) Crystal structure of the Type VIII clathrate, $Eu_8Ga_{16}Ge_{30}$. The framework ($[3^34^35^9]$; violet) is composed of Ge and Ga atoms. ($[A^x]$: A = number of vertices, x = number of faces).

In these cages, the guest atoms are thought to effectively "rattle" and scatter lattice phonons, suppressing the lattice thermal conductivity.[58] It has been observed that not only are the "rattling" atoms important, but that the open nature of the framework also results in low thermal conductivity.[59] A recent review[60] of this class of compounds provides a more detailed discussion of their synthesis and properties.

In the last decade research in this relatively large class of materials has accelerated. Electronic band structure calculations using density function theory (DFT)[61] on Type I clathrates suggested that ZT values of optimized compositions of $Sr_8Ga_{16}Ge_{30}$[62] and $Ba_8In_{16}Sn_{30}$ could reach 0.5 at room temperature and 1.7 at 800 K. Seebeck coefficient and resistivity measurements on polycrystalline samples[63] of $Ba_8Ga_{16}Ge_{30}$, $Ba_8Ga_{16}Si_{30}$, $Ba_8Ga_{16}Sn_{30}$, $Sr_8Ga_{16}Ge_{30}$, and $Ba_8Ga_{16}Ge_{30}$ above room temperature, combined with estimated high-temperature thermal conductivity from published results on $Ba_8Ga_{16}Ge_{30}$ and $Ba_8Ga_{16}Si_{30}$ were reported to yield $ZT = 0.7$ at 700 K and $ZT = 0.87$ at 870 K respectively.

Recent research for optimizing the thermoelectric properties of Type I clathrates above room temperature yielded promising results. A Czochralski grown $Ba_8Ga_{16}Ge_{30}$ crystalline ingot showed a Seebeck coefficient of -45 to $-150\ \mu V\,K^{-1}$ and electrical conductivity 1500 to 600 S/cm at 300 to 900 K. The thermal conductivity of this sample decreased from $1.8\ W\,m^{-1}\,K^{-1}$ at 300 K to $1.25\ W\,m^{-1}\,K^{-1}$ at 900 K, which gave rise to ZT of 1.35 at 900 K without passing through a maximum[64] (Figure 6 and 7). A repeated experiment reported a maximum giving $ZT \approx 0.9$ at 1000 K,[65] indicating the Czochralski prepared $Ba_8Ga_{16}Ge_{30}$ is a promising candidate for high-temperature thermoelectric applications. The high cost of gallium and germanium, however, will limit and actual commercial applications of this material.

The Type III clathrate structure formulated as $X_{24}E_{100}$ is composed of three kinds of cages namely E_{20} pentagonal dodecahedra, open dodecahedra, and distorted cubes. The n-

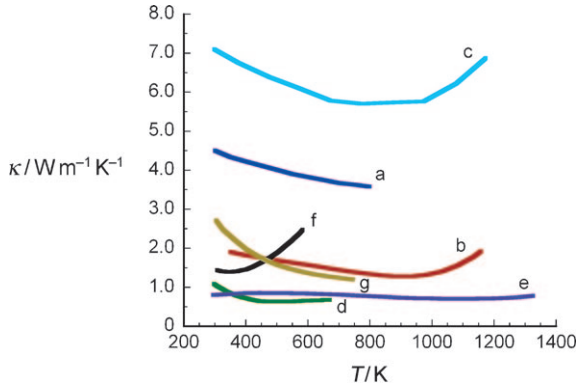

Figure 6. Comparison of total thermal conductivity as a function of temperature for a) $Ba_{0.3}Ni_{0.05}Co_{3.95}Sb_{12}$, b) $Ba_8Ga_{16}Ge_{30}$, c) $Hf_{0.75}Zr_{0.25}NiSn_{0.975}Sb_{0.025}$, d) β-$Zn_4Sb_3$, e) $Yb_{14}MnSb_{11}$, f) Bi_2Te_3, and g) PbTe.

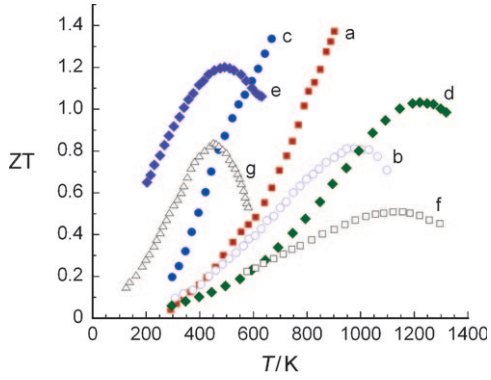

Figure 7. Variable temperature figure of merit (ZT) of a) $Ba_8Ga_{16}Ge_{30}$, b) $Hf_{0.75}Zr_{0.25}NiSn_{0.975}Sb_{0.025}$, c) β-$Zn_4Sb_3$, d) $Yb_{11}MnSb_{14}$, e) TAGS, f) $Si_{1-x}Ge_x$, and g) PbTe.

type optimized clathrate $Ba_{24}Ga_xGe_{100-x}$ ($x = 15$) was reported to reach ZT = 1.25 at 670 °C with a power factor of 1.15×10^{-3} W m^{-1} K^{-2} and a temperature-independent thermal conductivity of approximately 0.85 W m^{-1} K^{-1}.[66]

Future studies should also focus on other clathrate structure types, for example, Type VIII clathrate $Eu_8Ga_{16}Ge_{30}$ (Figure 5b). The Type I structure $Eu_8Ga_{16}Ge_{30}$ showed ZT ≈ 0.4 both in n- and p-type doped state at 400 K.[67] The Type VIII analogue of $Eu_8Ga_{16}Ge_{30}$ also showed ZT ≈ 0.3 at 400 K when n-type doped.[68] Interestingly, a ZT ≈ 1.2 at the same temperature was estimated by theoretical predictions for this Type VIII material when optimally p-type doped.[69]

3.1.3. *Half-Heusler Intermetallic Compounds*

Another class of compounds of considerable interest as potential thermoelectric materials for high-temperature applications are the half-Heusler (HH) intermetallic compounds formulated as MNiSn (M = Ti, Hf, Zr). HH phases have the MgAgAs[70] crystal structure which consists of three filled interpenetrating fcc sublattices and one vacant sublattice. The general formula is XYZ, where X and Y are transition metals and Z is a main-group element.[71] They are relatively easily synthesized. Another advantage of these compounds is their high melting points of 1100–1300 °C as well as their chemical stability with essentially zero sublimation at temperatures near 1000 °C. Figure 8 shows the unit cell

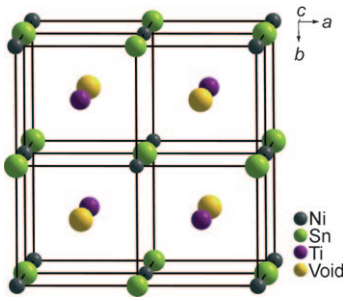

Figure 8. Crystal structure of the half-Heusler, TiNiSn, in a unit cell of cubic structure ($a = 5.9210$ Å). For clarity the void space is filled with void atoms in yellow.

of TiNiSn, in which Ti and Sn occupy a NaCl lattice and Ni occupies an fcc sublattice. The Heusler intermetallic compounds with fully filled sublattices are metals (full-Heusler alloys),whereas the vacant Ni atom sites in half-Heusler compounds give rise to narrow bands resulting in d-orbital hybridization and substantial semiconducting character of the compounds.[71–74] The rather narrow bands give rise to a large effective mass in these compounds and a large thermopower.[75]

The three filled sublattices are independently subject to chemical manipulation to optimize the thermoelectric properties of the compounds. For example, doping on the Sn site provides the charge carriers, while doping the Ti and Ni sites causes mass fluctuation disorder that can lead to the reduction of thermal conductivity. The most attractive feature of half-Heusler alloys as promising thermoelectric materials is the large room-temperature Seebeck coefficient of approximately 100 μV K^{-1} and high electrical conductivities of around 1000–10000 S cm^{-1}.[75–79]

Several half-Heusler alloys[75–78,80,81] have been investigated to improve their thermoelectric properties and ZnNiSn is the most intensively investigated member. Sb-doped TiNiSn alloys have power factors as high as 70 μW cm^{-1} K^{-2} at 650 K.[77] Despite the large power factor, a thermal conductivity of approximately 10 W m^{-1} K^{-1} is too high and results in a ZT of only 0.45 at 650 K.

Notable progress was reported with ZT ≈ 0.7 at 800 K for n-type $Zr_{0.5}Hf_{0.5}Ni_{0.8}Pd_{0.2}Sn_{0.99}Sb_{0.01}$.[81] Sakurada and Shutoh reported a ZT value near 1.4 at 700 K for n-type $(Zr_{0.5}Hf_{0.5})_{0.5}Ti_{0.5}NiSn_{1-y}Sb_y$.[80] Attempts to reproduce this result failed, but this report has drawn considerable interest to half-Heusler compounds as promising thermoelectric materials. Recently, approximately 30 half-Heusler compounds obeying the 18 valence-electron count were studied theoretically to predict thermoelectric performance through electronic structure and ab intio calculations.[82] It was predicted that several Co-, Rh-, and Fe-based half-Heusler compounds may be promising p-type materials whereas

LaPdBi and several others may be n-type with large power factors.

Increased atomic disorder at the transition-metal sites in half-Heusler alloys with different elements reduces the lattice thermal conductivity through induced mass fluctuations and strain field effects.[81,83] The room-temperature thermal conductivity ($\kappa \approx 7.1\ W\,m^{-1}\,K^{-1}$) for $Hf_{0.75}Zr_{0.25}NiSn_{0.975}Sb_{0.025}$, Figure 6c, is reduced from the $11.14\ W\,m^{-1}\,K^{-1}$ of ZrNiSn. If Ti is also added to the transition-metal site ($Hf_{0.60}Zr_{0.25}Ti_{0.15}NiSn_{0.975}Sb_{0.025}$), a further reduction to $6.4\ W\,m^{-1}\,K^{-1}$ was observed. With Pd substitution at the Ni site ($Hf_{0.75}Zr_{0.25}Ni_{0.9}Pd_{0.1}Sn_{0.975}Sb_{0.025}$) a value of $6.1\ W\,m^{-1}\,K^{-1}$ was reported.[84] However, at temperatures over 1000 K the thermal conductivity is increased through the onset of ionic thermal conduction within the open crystal structure.

For MNiSn half-Heusler alloys, Sb doping at the Sn site also increased the ZT value. For example, the ZT value of $Hf_{0.75}Zr_{0.25}NiSn_{0.975}Sb_{0.025}$ reached 0.81 at 1025 K and 0.78 at 1070 K, Figure 7b. This is because higher Sb content shifts the Seebeck coefficient maximum to higher temperature and leads to a larger power factor. Other members of the half-Heusler family with semiconducting properties include the (RE)MSb[79,85] (M = transition metal, RE = rare-earth metal) which are less-well studied but interest in these is increasing.

3.1.4. β-Zn_4Sb_3

β-Zn_4Sb_3 is a promising p-type compound at moderate temperatures which exhibits exceptionally low thermal conductivity.[86] The crystal structure of β-Zn_4Sb_3 is hwon in Figure 9, and has one Zn site and two independent Sb sites

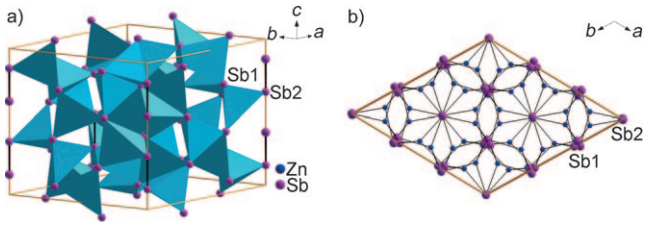

Figure 9. The crystal structure of β-Zn_4Sb_3 consists of a) three-dimensional corner-sharing tetrahedra of [$ZnSb_4$] units and b) Sb2 dimers which form in the octahedral holes within the distorted hexagonal Sb1 channels (view down to the *c* axis).

(the Sb1 and Sb2 sites are Sb^{3-} and Sb_2^{4-} dimers). One site is disordered with Zn and has lead to controversy in determining the true stoichiometry of the compound. The most recent structural analysis by X-ray single-crystal diffraction and powder synchrotron radiation diffraction reported that the structure includes three different interstitial sites in addition to the Zn site which is only 90% occupied and the final refined composition is $Zn_{12.8}Sb_{10}$.[87,88] Electronic structure and transport calculations using the crystal structure most recently identified have proposed the compound as a p-type semiconductor,[88] which was experimentally confirmed. It was also proposed by the calculation results that the Zn interstitial atoms play a dual role as electron donors and thermopower enhancers.

The highest ZT value reported for β-Zn_4Sb_3 is 1.3 at 670 K,[89] see Figure 7c, but apparently a critical drawback of β-Zn_4Sb_3 for a good thermoelectric material is that decomposition into ZnSb and Zn occurs before reaching its melting temperature of 841 K. The power factor of β-Zn_4Sb_3 is only moderate ($13\ \mu W\,cm^{-1}\,K^{-1}$ at 400 °C) for a high-ZT material,[89] compared with that ($70\ \mu W\,cm^{-1}\,K^{-2}$ near 400 °C)[77] of half-Heusler alloys. Therefore, the high ZT value of β-Zn_4Sb_3 is apparently associated with its "phonon-glass" behavior which gives rise to an unusually low thermal conductivity of approximately $0.9\ W\,m^{-1}\,K^{-1}$ at room temperature,[87] see Figure 6d. The interstitial atoms mentioned above are probably responsible for the glass-like phonon damping that suppresses the lattice thermal conductivity.

Doping in β-Zn_4Sb_3 leads to a further decrease in thermal conductivity[87,90] but the doping concentrations are limited. Even with the isostructural compound Cd_4Sb_3, the solid-solution of $(Zn,Cd)_4Sb_3$ forms below 6 mol% Cd_4Sb_3 at 400 °C.[91] No significant improvement in ZT of 1.3 at 670 K has been achieved for the doped samples.

3.1.5. The Zintl Phase $Yb_{14}MnSb_{11}$

$Yb_{14}MnSb_{11}$ has emerged recently as a promising intermetallic thermoelectric material for very high temperatures. The compound belongs to the Zintl family, $A_{14}MPn_{11}$, where A is an alkaline-earth or rare-earth metal, M is a transition or main-group metal, and Pn is a pnicogen, several members of which have been extensively studied for their magnetic properties.[92] The Yb analogue appears to be an excellent p-type thermoelectric material. Figure 10 shows the cubic structure of $Yb_{14}MnSb_{11}$ which crystallizes in the complex structure of $Ca_{14}AlSb_{11}$. It consists of one $[AlSb_4]^{9-}$ tetrahedron, one $[Sb_3]^{7-}$ polyatomic anion, four Sb^{3-} anions situated between $[AlSb_4]^{9-}$ and $[Sb_3]^{7-}$ units, and 14 Ca^{2+} per formula. $Yb_{14}MnSb_{11}$ is considered to be a valence precise semiconductor based on the classical Zintl concept in which the strongly electropositive Yb atoms donate electrons to Sb atoms in the structure. In reality, the material exhibits weakly metallic or semimetallic behavior as a function of temperature.

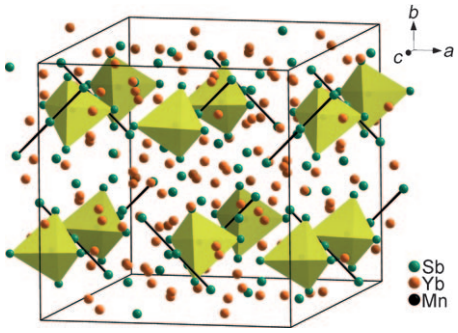

Figure 10. The cubic crystal structure of $Yb_{14}MnSb_{11}$ consists of one $[MnSb_4]^{9-}$ tetrahedral unit (yellow), one $[Sb_3]^{7-}$ ion (centers linked by black lines), four Sb^{3-} ions situated between the $[MnSb_4]^{9-}$ and $[Sb_3]^{7-}$ units, and 14 Yb^{2+} ions per formula.

Hot-pressed pellets of $Yb_{14}MnSb_{11}$ showed electrical conductivity and Seebeck coefficient of 185 $S\,cm^{-1}$ and 180 $\mu V\,K^{-1}$, respectively, at 1200 K. Despite the low power factor of approximately 6 $\mu W\,cm^{-1}\,K^{-2}$ for this material, the significantly low thermal conductivity in the rang 0.7–0.9 $W\,m^{-1}\,K^{-1}$ in temperatures between 200–1275 K gives rise to the remarkable ZT of approximately 1.0 at 1200 K,[93] see Figure 6e and 7d. The low thermal conductivity is primarily attributed to the large lattice constant, the structural complexity, and to the ionic character bonding in the lattice. $Yb_{14}MnSb_{11}$ has nearly twice the ZT at high temperatures (975–1275 K) as a p-type SiGe based material (maximum $ZT \approx 0.6$ at 873 K).[94,95] The only other material system that has any appreciable ZT at 1200 K is the Si-Ge alloy in the radioisotope thermoelectric generator (RTG) for deep-space probes. So it is possible that $Yb_{14}MnSb_{11}$ and its alloys may replace p-type Si-Ge alloys in future missions.

A variety of substitutions in $Yb_{14}MnSb_{11}$ with other alkaline-earth and rare-earth metals as well as transition/main-group metals has been achieved for further optimization of the thermoelectric performance.[96,97] Studies of the charge-transport properties of $Yb_{14}MnSb_{11}$ under pressure showed that the conductivity decreased and thermopower increased with increasing pressure.[98] The room-temperature ambient-pressure conductivity and Seebeck coefficient, 689 $S\,cm^{-1}$ and 47 $\mu V\,K^{-1}$, of single-crystal samples increased to 645 $S\,cm^{-1}$ and 55 $\mu V\,K^{-1}$ under 2.3 GPa.

3.1.6. Metal Oxides

An intriguing newcomer to the field of thermoelectrics is the class of metal oxides. Although many metal oxides had been screened for high power factor, the results were discouraging. However, the ternary and quaternary cobaltates have generated much excitement because of their high thermopower and related high power factor coupled with a low thermal conductivity.

The appeal of oxides for high-temperature thermoelectric power generation derives from their presumed high thermal and chemical stability in air. In general, most oxides are known to be poor conductors with low charge-carrier mobility. The layered $NaCo_2O_4$ has a large enough thermopower and metal-like conductivity to place it on par with many other interesting candidates discussed herein.[99] The proposed origin of the unusually large thermopower of $NaCo_2O_4$ is a large entropy of $k_B \ln 6$, which is equivalent to 150 μV/K at the high-temperature limit, and is caused by the low-spin state Co^{4+}.[100,101] The thermopower and conductivity of $NaCo_2O_4$ single crystals reach 100 $\mu V\,K^{-1}$ and 5000 $S\,cm^{-1}$ at 300 K, consequently the power factor is 50 $\mu W\,cm^{-1}\,K^{-2}$. $ZT \approx 0.8$ at 1000 K from a polycrystalline sample[102,103] and $ZT > 1$ at 800 K from a single-crystal sample[104] have been reported.

The structure of $NaCo_2O_4$ is shown in Figure 11, the CdI_2-type CoO_2 layer is formed by edge-sharing distorted octahedra and Na^+ ions randomly occupy 50 % of the interlayer sites. The $[CoO_2]^{0.5-}$ sheets are a strongly correlated electron system. The sheets serve as electronic-transport layers and the intercalated Na^+ ions serve as the phonon-scattering region to give low thermal conductivity (approximately 3 $W\,m^{-1}\,K^{-1}$ at room temperature).[105,106]

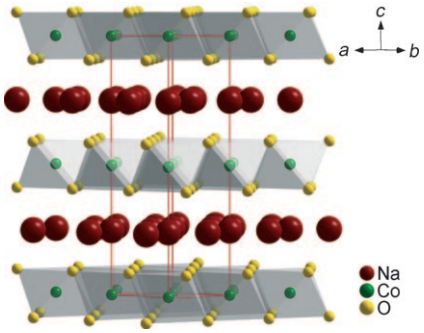

Figure 11. The crystal structure of $NaCo_2O_4$ is composed of $[CoO_2]^-$ ionic layers and Na^+ ions which occupy half of the interlayer atomic sites. The Co ions $[CoO_2]^-$ in the layers have an octahedral coordination environment and adopt the CdI_2 structure type.

Several derivatives including bismuth-doped $Ca_3Co_4O_9$ ($ZT > 1$ at 1000 K),[107] $(Bi,Pb)_2Sr_2Co_2O_8$,[108–110] $TlSr_2Co_2O_y$,[111] and $(Hg,Pb)Sr_2Co_2O_y$[112] showed good p-type thermoelectric performance. All these materials have a common structural feature which is the CoO_2 layer. This layer seems to be a key ingredient for their good thermoelectric performance. Thus, the transport properties of these oxides are proposed to be associated with a block layer concept which is often applied in high-temperature superconductors. The best ZT values reported for p-type oxides are given in Figure 12.[113]

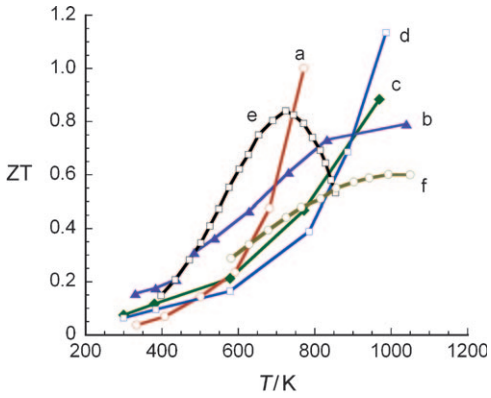

Figure 12. The figure of merit (ZT) for promising oxides as a function of temperature, a) Na_xCoO_2 (crystal), b) Na_xCoO_2 (ceramic), c) $Ca_3Co_4O_9$ (crystal), and d) $Bi_2Sr_2Co_2O_y$ (crystal) compared with conventional materials, e) PbTe and f) $Si_{1-x}Ge_x$.

Corresponding oxides with good n-type thermoelectric properties have not yet been discovered. The best n-type oxides to date are $SrTiO_3$, heavily doped with Nb and La, which show $ZT \approx 0.37$ and 0.26 at 1000 K,[114] respectively. These materials have high power factors near 20 $\mu W\,cm^{-1}\,K^{-2}$ but a very high thermal conductivity of 10 $W\,m^{-1}\,K^{-1}$ at 300 K. Al-doped ZnO ($Al_{0.02}Zn_{0.98}O$) has been reported with comparable a ZT value ($ZT \approx 0.3$ at 1000 K).[115,116] From room temperature to 1000 K this material shows n-type metallic

behavior with considerably higher power factor of approximately 8–15 $\mu W\,cm^{-1}\,K^{-2}$ and high thermal conductivity of 40–5 $W\,m^{-1}\,K^{-1}$. Another form of Al-doped ZnO was reported with the enhanced ZT of 0.4 at 500 °C which was achieved by applying a void forming agent (VFA), such as nanoscale particles of carbon or organic polymer.[117] An n-type composite phase, Ca-doped $(ZnO)_3(In_2O_3)$, fabricated by the reactive templated grain growth (RTGG) method was reported with $ZT \approx 0.31$ at 1053 K.[118]

Serious drawbacks currently in constructing modules with oxide materials are the high contact resistance at the junction of oxide/metal electrode and cracking/exfoliation during operation cycles. The cracking/exfoliation comes from a significant difference in thermal expansion between them.[119]

3.1.7. $FeSb_2$

$FeSb_2$ is of interest because of its record high Seebeck coefficient ($-45\,000\ \mu V\,K^{-1}$) at low temperatures (ca. 10 K) resulting in the largest power factor ever reported (ca. 2300 $\mu W\,cm\,K^{-2}$).[120] This power factor is 65-times larger than that of Bi_2Te_3. $FeSb_2$ is one of two phases in the Fe-Sb system and crystallizes in the marcasite crystal structure. According to magnetic susceptibility, Mössbauer effect, resistivity, and Seebeck coefficient measurements $FeSb_2$ is described as a strongly correlated electron system. Band-structure calculations show localized Fe d-states in the valence band of the compound[121] that are expected to contribute to the large experimental Seebeck coefficient because S is dependent on the variation of the DOS near the Fermi energy. The drawback of $FeSb_2$ is its large lattice thermal conductivity which prevents a significant figure of merit ZT. At 12 K the resulting ZT is only 0.005.[120] Attempts to substitute Sb with Sn were unsuccessful in increasing ZT.[121] The possible existence of a very narrow band, formed by Fe 3d states weakly hybridized with Sb 5p states was suggested, and that the coherence of this band begins to deteriorate as the temperature increases above 10 K. The appearance of a colossal Seebeck coefficient within the "very narrow band" scenario is worthy of further exploration as any new insights obtained in this regard would help identify other more promising colossal power-factor materials with Seebeck maxima at higher temperatures. This phenomenon offers a challenge for future theoretical work.

3.2. Chalcogenide Compounds

Chalcogenide compounds comprise a large class of materials that are predominantly semiconductors. Generally, they are air stable, melt congruently, and have high melting points. The compounds have many of the desirable attributes for promising thermoelectric materials. Because of their versatility in combination with other elements and the small variation in electronegativity between sulfur, selenium, and tellurium, it is possible to obtain semiconductors with energy gaps appropriate for thermoelectric applications (e.g. 0.1–0.8 eV) over a wide range of temperature. The class of chalcogenide materials has had a prominent position in the field of thermoelectricity going back to its early stages. The cornerstone of today's thermoelectric cooling technology, for example, has been Bi_2Te_3 and its solid solutions $Bi_{2-x}Sb_xTe_3$ (p-type) and $Bi_2Te_{3-x}Se_x$ (n-type).[122] For over forty years this system has been responsible for the continued interest and development of this field. Another important chalcogenide is PbTe which has a maximum $ZT \approx 0.8$ at approximately 770 K, and has been suitable for power generation at intermediate temperatures. The germanium-based TAGS (Te-Ag-Ge-Sb) are more efficient than PbTe but have found little use due to their high sublimation rate, high cost, and the presence of a low-temperature phase transition.[123]

3.2.1. Anisotropic Materials

3.2.1.1. Tl_9BiTe_6, Ag_9TlTe_5, and Tl_2SnTe_5

Thallium chalcogenides have very low thermal conductivity and high Seebeck coefficients but relatively low electrical conductivity. It was predicted that the carrier concentration could be controlled by using doping to improve the power factor,[124] but attempts to do this have not been reported. Nevertheless, Tl_9BiTe_6, Tl_2SnTe_5, and Ag_9TlTe_5 are noteworthy phases as promising thermoelectric materials.

Tl_9BiTe_6 is a derivative of the isostructural compound Tl_5Te_3 formed by replacing Tl^{3+} with Bi^{3+} in $2[Tl_5Te_3] = [Tl^+_8(Tl^+Tl^{3+})Te^{2-}_3]$. As shown in the coordination polyhedra in Figure 13a, the nearest neighbors of the Te atoms are

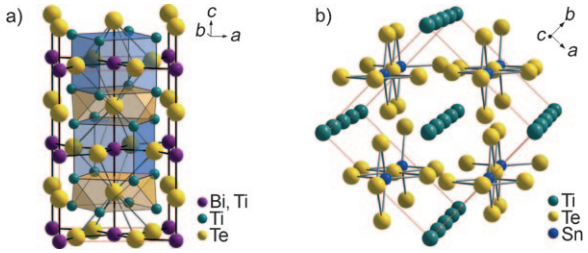

Figure 13. a) The crystal structure of Tl_9BiTe_6; the heavy-atom site disordered being occupied by Bi and Tl. There are two alternating cages of Tl atoms (yellow and blue). b) The crystal structure of Tl_2SnTe_5 is composed of tetrahedral $[SnTe_4]$ units bridged by Te atoms in square-planar geometry.

exclusively Tl atoms and the central position surrounded by Te atoms in the octahedral pocket is equally occupied by Tl and Bi. Tl_9BiTe_6 was reported to exhibit a thermoelectric figure of merit of $ZT \approx 1.2$ at 500 K, mainly arising from the remarkably low lattice thermal conductivity of Tl_9BiTe_6 of approximately 0.39 $W\,m^{-1}\,K^{-1}$ at 300 K (Figure 14a).[125]

Tl_2SnTe_5 is a tetragonal phase with infinite chains of $[SnTe_5]^{2-}$ running parallel to each other and eightfold coordinate Tl^+ ions between the channels (Figure 13b). One of the main reasons for the very low lattice thermal conductivity (0.5 $W\,m^{-1}\,K^{-1}$) of this compound is relatively long Tl–Te bonds which produce very low frequency phonons. This compound could be optimized to $ZT \approx 1$ at 500 K.[126]

Ag_9TlTe_5 is isostructural to Ag_2Te, which has an even lower lattice thermal conductivity than Tl_2SnTe_5.[127,128]

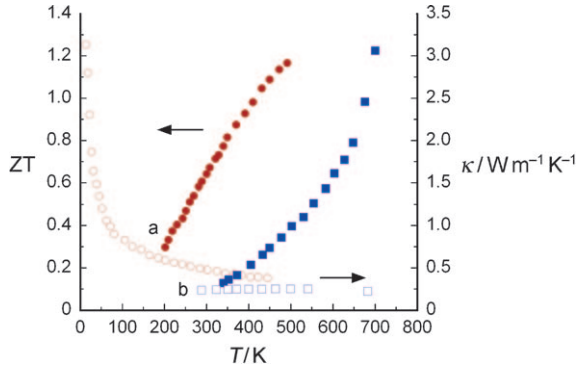

Figure 14. Variable temperature figure of merit (ZT; solid symbols) and thermal conductivity (open symbols) for Tl_9BiTe_6 (circle) and Ag_9TlTe_5 (square).

Ag_9TlTe_5 combines extremely low thermal conductivity of 0.22 $W m^{-1} K^{-1}$ and relatively low electrical resistivity to give ZT = 1.23 at 700 K (Figure 14b).

Another interesting thallium-containing compound is $TlIn_{1-x}Yb_xTe_2$. The solid solutions of $TlInTe_2$-$TlYbTe_2$ are p-type and have a notably high ZT value at 500–700 K. For a single crystal of $TlIn_{0.94}Yb_{0.06}Te_2$ grown by float-zone melting, physical properties at 700 K of $Z = 2.61 \times 10^{-3} K^{-1}$, thermopower of approximately 630 $\mu V K^{-1}$, electrical conductivity of approximately 39.5 $S cm^{-1}$, and lattice thermal conductivity of approximately 0.61 $W m^{-1} K^{-1}$ were reported.[129] Despite the apparently promising thermoelectric properties of this class of materials, no further report has followed.

Because of significant toxicity and environmental issues, thallium-containing compounds are unlikely to be accepted for practical use. Despite this, studies on this class of compounds are important from a scientific point of view because they could provide a great deal of insights on how to reduce thermal conductivity and optimize the ZT values of materials.

3.2.1.2. *Alkali-Metal Bismuth Chalcogenides*

During the last decade much interest has developed in the chemistry of bismuth chalcogenides owing to their potential as thermoelectric materials as well as the abundance of new compounds discovered in this area. Some of the new compounds include KBi_3S_5,[130] $KBi_{6.33}S_{10}$,[131,132] $K_2Bi_8S_{13}$,[131,133,134] α-,β-$K_2Bi_8Se_{13}$,[135,136] $K_{2.5}Bi_{8.5}Se_{14}$,[136] $A_xBi_4Se_7$[137] ($x = 1$, 2), $BaBiTe_3$,[138] $CsBi_4Te_6$,[139] $ALn_{1\pm x}Bi_{4\pm x}S_8$[140] (A = K, Rb; Ln = La, Ce, Pr, Nd), $BaLaBi_2Q_6$[141] (Q = S, Se), α-,β-$APbBi_3Se_6$[142] (A = K, Rb, Cs), $K_{1-x}Sn_{5-x}Bi_{11+x}Se_{22}$,[143] $A_{1+x}M'_{4-2x}Bi_{7+x}Se_{15}$[144] (A = K, Rb; M′ = Sn, Pb), $Sn_4Bi_2Se_7$,[145] $SnBi_4Se_7$,[146] $CdBi_2S_4$,[147] $CdBi_4S_7$,[147] $Cd_{2.8}Bi_{8.1}S_{15}$,[147] $Cd_2Bi_6S_{11}$,[147] $Ba_3Bi_{6.67}Se_{13}$,[148] and $Ba_3MBi_6Se_{13}$[148] (M = Sn, Pb). These types of compounds have shown low thermal conductivity, high thermopower, and often high electrical conductivity,[133,134,149,150] reaching, in the case of $CsBi_4Te_6$, a ZT value of 0.8 at 225 K (see Section 3.2.1.4).

The common feature of these materials is their high structural anisotropy. The bismuth chalcogenide frameworks derive from condensing Bi-Q octahedra through the sharing of edges to form blocks that consist of the NaCl-, Bi_2Te_3-, CdI_2- and Sb_2Se_3-type structure. These octahedral blocks come in different shapes and sizes and are usually connected either directly with each other or through metal atoms of high (>6) coordination number. Many of the compounds are members of large homologous series which are defined by these adjustable blocks while following the same assembly principle. These characteristics point to a seemingly countless number of novel phases that can potentially form. The features mentioned above can generate chemical and structural complexity, diversity, and disorder that can be desirable in good thermoelectric materials.[2,19,151]

3.2.1.3. *β-$K_2Bi_8Se_{13}$*

One of the most noteworthy phases is β-$K_2Bi_8Se_{13}$ which shows promising thermoelectric properties by virtue of its very low thermal conductivity and relatively high power factor.[136] Doping studies on this system have shown that its ZT value can be substantially improved.[136,152]

β-$K_2Bi_8Se_{13}$ has a low-symmetry monoclinic structure[136] that includes two different interconnected Bi/Se building blocks (the so-called $NaCl^{(100)}$- and $NaCl^{(111)}$-type) and K^+ ions in the channels (Figure 15). These two Bi/Se blocks are infinitely extended along the crystallographic *b*-axis and connected to each other at special mixed-occupancy K/Bi sites. Its highly anisotropic structure is reflected by the formation of needle-shaped crystals.

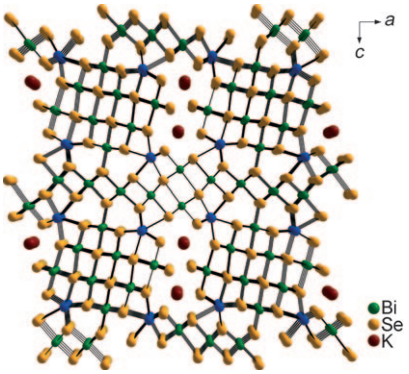

Figure 15. Crystal structure of β-$K_2Bi_8Se_{13}$ viewed down to the *b* axis. The structure consists of two Bi/Se building blocks (NaCl type and Bi_2Se_3 type) connected at the K/Bi mixed site (blue), the K atoms are in the channels.

Charge-transport and thermal-conductivity measurements on β-$K_2Bi_8Se_{13}$ single crystals showed low thermal conductivity (ca. 1.3 $W m^{-1} K^{-1}$) and a relatively high power factor ($S^2\sigma \approx 10$ $\mu W cm^{-1} K^{-2}$) at room temperature, giving ZT = 0.22, (Figure 16).[136] The Seebeck coefficient is negative indicating n-type character. The material is typically obtained as a highly degenerate semiconductor. Based on β-$K_2Bi_8Se_{13}$, solid solutions with the isostructural compounds $K_2Sb_8Se_{13}$, $Rb_2Sb_8Se_{13}$, and $K_2Bi_8S_{13}$ have been studied.[153–158] A substantial improvement (by a factor of 2.5) of the power factor

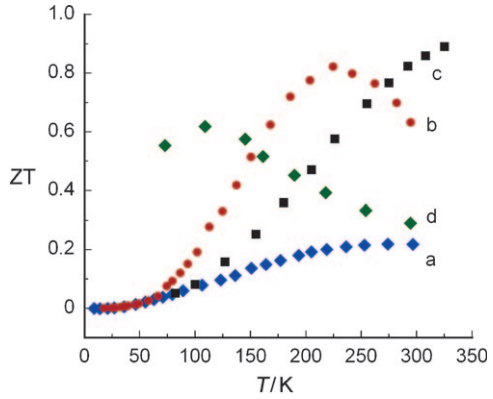

Figure 16. Temperature-dependant figure of merit (ZT) for a) β-$K_2Bi_8Se_{13}$, b) $CsBi_4Te_6$, and for comparison c) Bi_2Te_3 and d) BiSb alloy.

at high temperature with slightly reduced thermal conductivity ($\kappa \approx 1.08\ W\,m^{-1}\,K^{-1}$) was reported for polycrystalline samples of 0.2% Sn doped $K_2Bi_{8-x}Sb_xSe_{13}$ ($x = 1.6$).[153] A ZT of approximately 1 at 700–800 K is possible in these systems. The charge-transport properties have also been studied under pressure, where a significant increase in the power factor as well as a peak in the Seebeck coefficient was observed, suggesting electronic topological transition upon compression.[159]

A mixed-occupancy K/Bi disorder at the sites bridging two different structural units is a very common feature in the alkali-metal bismuth selenide system. Electron-diffraction and charge-transport properties in conjunction with Hall coefficient measurements on a series of solid solutions, $K_2Bi_{8-x}Sb_xSe_{13}$ and $K_{2-x}Rb_xBi_8Se_{13}$, suggest that the degree of disorder at the mixed occupancy K(Rb)/Bi(Sb) sites is very important affecting the thermoelectric properties.[154] This idea is supported by the results of ab initio density functional theory band-structure calculations on this compound.[160] Therefore, gaining control of these sites could hold the key in further optimizing the thermoelectric properties in these systems.

3.2.1.4. $CsBi_4Te_6$

$CsBi_4Te_6$ is a promising material for low-temperature thermoelectric applications. This compound features a strong anisotropic structure that contains both formally Bi^{3+} and Bi^{2+} centers. The unusual reduced Bi^{2+} centers form Bi–Bi bonds of 3.238 Å. The compound has a lamellar structure with slabs of $[Bi_4Te_6]^-$ alternating with layers of Cs^+ ions (Figure 17). Extensive studies showed that $CsBi_4Te_6$ was very responsive to the type and level of doping agents and could produce both p- and n-type materials.[161] The presence of Bi–Bi bonds in the structure is responsible for the very narrow energy gap (ca. 0.08 eV),[161–163] nearly half of that of Bi_2Te_3. The narrower band gap is responsible for the maximum ZT value in $CsBi_4Te_6$ being at lower temperatures than in Bi_2Te_3. Different dopings of the p-type $CsBi_4Te_6$ give high values of power factor ($> 30\ \mu W\,cm^{-1}\,K^{-2}$) between 100 and 220 K. Materials doped with Sb, Bi, SbI_3, and BiI_3 have highest power factors of 40–60 $\mu W\,cm^{-1}\,K^{-2}$ at 150–180 K. A ZT value of 0.8 at 225 K

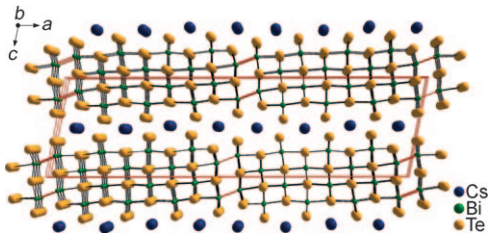

Figure 17. Crystal structure of $CsBi_4Te_6$ viewed down to the *b* axis. Cs atoms are located between NaCl-type Bi/Te layers which are composed of $[Bi_4Te_6]^-$ building units interconnected by Bi–Bi bonds (red).

was obtained for 0.06% SbI_3-doped $CsBi_4Te_6$ (Figure 16).[139] For n-materials generated by In_2Te_3- and Sn-doping, power factors of near 25 $\mu W\,cm^{-1}\,K^{-2}$ were obtained at 100–150 K.

Band calculations[164] for $CsBi_4Te_6$ suggest that this material has electronic structural features that are highly advantageous for good thermoelectric properties. The proposed key feature leading to the high ZT value of $CsBi_4Te_6$ is a large anisotropy in the effective mass. This proposal is supported by angle-resolved photoelectron spectroscopy studies (ARPES) for p-type $CsBi_4Te_6$.[162] Another report[163] on the band structure of $CsBi_4Te_6$ suggests that the carrier concentration of the best p-type $CsBi_4Te_6$ material ($ZT \approx 0.8$) is close to the optimal value achievable, but the thermoelectric properties of n-type $CsBi_4Te_6$, when optimally doped, may exceed those of the p-type doped materials. It would be interesting to experimentally investigate these predictions.

3.2.1.5. Bi_2Te_3

The scientific literature on this prototypical system is vast and it is not our intent to cover it.[6] Only the most recent developments will be mentioned. Bi_2Te_3 is a narrow-gap semiconductor with an indirect gap of approximately 0.15 eV. It crystallizes in the rhombohedral space group $R\bar{3}m$ the structure comprises plates, made up of five atomic layers (Te1-Bi-Te2-Bi-Te1), stacked by van der Waals interactions along the *c*-axis in the unit cell (Figure 18). The state-of-the-art Bi_2Te_3 materials with $ZT \approx 1$ are synthesized by alloying with Sb for p-type and Se for n-type materials. In actual

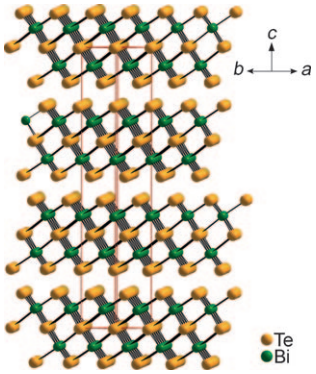

Figure 18. Crystal structure of rhombohedral Bi_2Te_3 with five atomic layers stacked along the *c* axis by van der Waals interactions. The Bi atoms are coordinated with six Te atoms in octahedral geometry.

devices the p-type "legs" are generally hot-pressed and annealed pellets of $Bi_{2-x}Sb_xTe_3$ ($x \approx 1.5$) which have good mechanical properties. The n-type counterpart is typically an ingot form of $Bi_2Te_{3-y}Se_y$ ($y \approx 0.3$) grown by zone melting techniques.

Superlattice systems with low dimensionality have been proposed as a means to greatly enhance the thermoelectric ZT value as a result of the confinement effects on the electronic density of states. A ZT of 2.4 at room temperature[165] was claimed for a p-type Bi_2Te_3/Sb_2Te_3 superlattice grown by chemical-vapor deposition, a value which purportedly broke through the long-standing $ZT \approx 1$ record for Bi_2Te_3 alloys. It was proposed that the extraordinarily high ZT value of 2.4 (in the direction perpendicular to the layers of Bi_2Te_3) in these artificially constructed systems originates from two factors: a) exceedingly low lattice thermal conductivity (ca. 0.24 $W m^{-1} K^{-1}$) and b) a cross-plane electron mobility which is equal to the in-plane electron mobility. This idea is very surprising because in pure Bi_2Te_3 the cross-plane mobility is less than half that of the in-plane mobility. It was proposed that the first factor derives from phonon back reflection at Bi_2Te_3/Sb_2Te_3 interfaces. The suggested reasons for the second factor involve the very small band offsets between the Bi_2Te_3 and Sb_2Te_3 slabs, but this argument leads to the conclusion that in pure Bi_2Te_3 the cross-plane mobility should also be equal to that of in-plane mobility since the valence-band offsets between Bi_2Te_3 slabs is zero. Validation of these extraordinary high ZT value results has not been reported. Detailed reviews of thin-film thermoelectric materials can be found elsewhere.[12,13,15]

Significant improvements in the ZT value of Bi_2Te_3-based bulk materials have been reported recently (Figure 19).[166–169] A quasi-layered nanotube n-type Bi_2Te_3 with a holey one-dimensional structure was prepared by hydrothermal synthesis and has $ZT \approx 1.0$ at 450 K.[166] Utilizing this technique, nanotubes embedded in a Bi_2Te_3 matrix, grown by the zone melting technique, was reported with a ZT value of 1.25 at 420 K and n-type properties.[167] Melt spinning followed by spark plasma sintering (SPS) gave p-type Bi_2Te_3 ingots with a ZT value of 1.35 at 300 K.[168] The material features 25 nm wide ribbons composed of nanostructured layers of Bi_2Te_3 crystals with 1 nm interplanar distance.

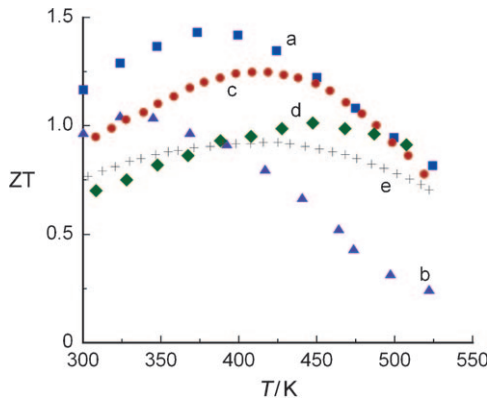

Figure 19. Figure of merit (ZT) as a function of temperature for bulk Bi_2Te_3 materials prepared by a) ball milling and hot pressing, b) zone melting, c) melt spinning and SPS, and d) hydrothermal synthesis, and for comparison e) the state-of-the-art Bi_2Te_3. The nanotube prepared by (d) is n-type and the others are p-type material.

The highest ZT value for a bulk p-type Bi_2Te_3 material was reported recently. The material with $ZT \approx 1.4$ at 100 °C was prepared by ball milling followed by direct-current hot pressing.[169] The ZT-value enhancement for this system appears arise from reducing the phonon thermal conductivity while maintaining a comparable power factor to that of the bulk p-type $Bi_{2-x}Sb_xTe_3$. This material is called "nanobulk" $Bi_{2-x}Sb_xTe_3$ and it is a single-phase material made of nanograins and macrograins mixed together. One issue that arises in a material such as this is the long-term stability of the nanograins against growth by grain–grain fusion at elevated temperatures.

3.2.2. Isotropic Materials

3.2.2.1. PbTe

PbTe is the premiere thermoelectric material for mid-range temperature (600–800 K) applications. It crystallizes in the NaCl crystal structure with Pb atoms occupying the cation sites and Te forming the anionic lattice. A band gap of 0.32 eV allows it to be optimized for power-generation applications and can be doped either n- or p-type with appropriate dopants. The maximum ZT value for PbTe has been reported to be 0.8–1.0 at approximately 650 K. The thermoelectric properties of PbTe are reasonably well understood and have been reviewed previously.[170,171] The lattice thermal conductivity of PbTe is approximately 2.2 $W m^{-1} K^{-1}$ at room temperature and falls at higher temperature with a $1/T$ dependence. Significant recent work has focused on improving the thermoelectric properties of PbTe by nanostructuring, as will be discussed in the following section, and more recently modification of the density of states to create resonance states in the conduction band thereby increasing the Seebeck coefficient. Additionally, recent work has also focused on understanding the mechanical properties of PbTe for device fabrication.[172–174]

Dopant atoms in a semiconductor can introduce electronic states that can resonate with the semiconductor matrix.[175–178] Based on a theoretical study of the effect of Group 13 dopants on the electronic structure of PbTe,[178] several different impurities were substituted in PbTe and $Pb_{1-x}Sn_xTe$. When $Pb_{1-x}Sn_xTe$ was doped with In, the resonance level of In was not appropriately located in the conduction or valence band and no enhancement in thermoelectric properties was observed.[179] However, when Tl was substituted in PbTe the resonant state was properly located in the valence band and the semiconductor could be p-type doped. This phenomenon was recently utilized effectively in the PbTe:Tl system where a large ZT value (1.5 at 773 K) was attributed to an increase in the Seebeck coefficient compared to that of PbTe.[180] The increase in the density of states was confirmed experimentally via optical spectroscopic measurements and low-temperature specific heat measurements. Additionally, the thermal conductivity in this system was not reduced compared to pristine PbTe. Thus if the resonant-state improvement could be coupled with a reduced thermal

conductivity, exceptional increases in ZT value may be obtained. Nanostructured versions of PbTe have very different thermal and charge-transport properties and are discussed in Section 3.3.5. Although nanostructuring has become a hot topic in PbTe-based materials, solid-solution alloying still remains an active area of research.[181,182]

3.2.2.2. $AgSbTe_2$

$AgSbTe_2$ is a p-type material with a high ZT value with reports claiming it to be as high as 1.3 at 720 K.[11] This material is the only ternary phase in the Ag-Sb-Te ternary phase diagram. The simple ternary stoichiometry is deceptive and hides an exceedingly complex structure that only recently has begun to be investigated in detail. The phase diagram of the Ag-Sb-Te system indicates that this compound is metastable at low temperatures and can be prone to decomposition to Ag_2Te and Sb_2Te_3.[183–185] Therefore most samples of $AgSbTe_2$ may actually be three-phase mixtures of $AgSbTe_2$/Ag_2Te/Sb_2Te_3. Indeed, structural studies indicate a complicated microstructure.[186]

$AgSbTe_2$ crystallizes in the rock salt structure. This implies that the Ag and Sb atoms are randomly distributed in the Na sites of rock salt structure, but recent studies showed evidence of Ag and Sb atom ordering in the structure. The existence of ordering is reasonable (in fact, it should be expected) because random occupation of the Na sites would create too many Ag^+–Ag^+ and Sb^{3+}–Sb^{3+} second-neighbor contacts in the lattice which are energetically unfavorable when compared to Ag^+-Sb^{3+} contacts. Because of the very similar scattering lengths of Ag, Sb, and Te atoms, ordering in $AgSbTe_2$ is difficult to detect with X-ray, neutron, or electron diffraction. Thus, although evidence of ordering has been detected, a unique ordering model based on structure refinement could not be found. Based on the available evidence to date, it is likely that the domains of $AgSbTe_2$ contain regions of ordered and disordered Ag and Sb atoms.

From the above it is evident that there are significant complications in the chemistry of $AgSbTe_2$ and this has been the root of considerable confusion as to the true nature of the structure, composition, and even whether it is a semiconductor or a semimetal.[187,188] For example, analysis of the temperature dependence of the resistivity suggests energy-gap values ranging from 0.6 to 0.2 eV. Galvanomagnetic and thermoelectric studies showed that some samples can have positive and others negative Hall coefficients while maintaining a positive Seebeck coefficient, which suggests strong sample to sample variability.[189] Given the thermodynamic instability of $AgSbTe_2$ suggested by its phase diagram it is clear that the synthesis and crystal-growth conditions strongly affect the nature of these samples.

First-principles calculations of the electronic, optical, and lattice vibrational properties of $AgSbTe_2$ performed with the generalized gradient approximation (GGA) show a negative band gap[190] (i.e. semimetal) but when the screened-exchange local-density approximation (sx-LDA) method is applied, it successfully corrects the band-gap problem found with GGA. sx-LDA suggests a vanishing density of states at the Fermi level, which is consistent with semiconducting behavior for $AgSbTe_2$.[191] Various optical properties, including the dielectric function, absorption coefficient, and refractive index, as functions of the photon energy are also calculated with the sx-LDA and are found to be in good agreement with experiments. The calculated phonon spectra show that the optical modes of $AgSbTe_2$ are very low in frequency and should scatter strongly with acoustic modes during heat transport. The scattering of acoustic phonons by optic modes and the possible Ag/Sb disorder may explain the extremely low lattice thermal conductivity of $AgSbTe_2$. This conclusion is not a clean one because the effect of the Ag_2Te and Sb_2Te_3 inclusions in the matrix of $AgSbTe_2$ mentioned above is not taken into account by these studies.

Recent experimental studies on $AgSbTe_2$ suggest it is a semiconductor with a very narrow energy gap of 7 meV, with highly mobile electrons that dominate the Hall measurements, and holes in a heavy band that dominate the thermoelectric power.[192,193] Since this gap energy is comparable to the thermal energy, $k_B T$, for temperatures above 100 K, it was suggested that $AgSbTe_2$ can in practice be considered as an indirect zero-gap material above that temperature. The synthetic details for the preparation of these samples were not reported.

3.2.2.3. $AgSbTe_2$/GeTe

The reaction of GeTe with $AgSbTe_2$ gives alloys of the form $(AgSbTe_2)_{1-x}(GeTe)_x$. These materials have been studied for several decades and they are commonly referred to by the acronym "TAGS-*m*", where *m* represents mole percent GeTe.[194] They are intrinsically p-type materials and are typically combined with a PbTe n-type leg in a thermoelectric device. The discovery of a high ZT value of approximately 1.4 and 1.5 at 750 K for $m = 80$ and 85, respectively,[195] motivated subsequent studies on the (GeTe)-rich compositions.[196] This was one of the first materials to exhibit $ZT > 1$ at high temperature and suggested that $ZT \approx 1$ was not necessarily a physical barrier of some sort as many had feared. TAGS-85 in fact has been used in NASA missions since the early 1970s. The TAGS system undergoes a polymorphic transformation at 510 K, from a low-temperature polar rhombohedral ($R3m$) to a high-temperature NaCl-type cubic ($Fm\bar{3}m$) structure.[197] The transition temperature depends primarily on the ratio of GeTe to $AgSbTe_2$ and the Sb:Ag ratio. Although twinning is pervasive in the rhombohedral structure, high-temperature X-ray diffraction and TEM analysis showed no evidence for any second phases, coherent or incoherent, in this composition.[197,198] In other words, the (GeTe):($AgSbTe_2$) system appears to be a proper solid solution although a recent report seems to indicate nanostructuring.[199]

As the composition is varied from $AgSbTe_2$ to GeTe in the solid solution, the transport properties vary smoothly, except for the double minimum observed in thermal conductivity at 80% and 85% GeTe. These minima result in an extremely low lattice thermal conductivity (0.3–1.0 $W m^{-1} K^{-1}$) while at the same time the materials exhibit a large carrier mobility, μ, of 100–200 $cm^2 V^{-1} s^{-1}$. ZT values as high as 1.7 were reported for the TAGS-80 composition.[200]

3.3. Inhomogeneous Nanostructured Materials

Theoretical work on reports of vastly improved ZT values in nanoscale materials grown by thin-film deposition techniques showed that these increases arose from reducing the thermal conductivity. However, the synthesis of large amounts of material through solid-state methods is desirable for widespread application. This situation prompted the exploration of new approaches and concepts for the preparation of nanostructured materials. The $AgPb_mSbTe_{m+2}$ (LAST-*m*) family of compounds and its p-type analogue $NaPb_mSbTe_{2+m}$ (SALT-*m*) for example, are inhomogeneous on the nanoscale and achieve large ZT values that can be attributed to substantial decreases in the thermal conductivity compared to PbTe. Additional methods to prepare nanostructured PbTe include precipitation and growth, spinodal decomposition, matrix encapsulation, and the preparation of nanoscale polycrystalline materials. Each of these materials and methods will be described in the following sections.

3.3.1. $AgPb_mSbTe_{2+m}$

PbTe has a number of derivatives that have shown some of the most promising results to date among bulk materials. The first system, $AgPb_mSbTe_{2+m}$ (LAST-*m*: lead antimony silver telluride), reported to achieve $ZT > 1$, derives from the combination of PbTe and $AgSbTe_2$. Early studies of this system reported it to be a solid solution between PbTe and $AgSbTe_2$ (both rock salt NaCl type structures) with p-type properties and an unusually low lattice thermal conductivity. The belief that the system is a solid solution came from the fact that the LAST-*m* series do follow Vegard's law when it comes to the dependence of the lattice constant with composition. The average solid solution structure is shown in Figure 20. Recent studies, however found that n-type samples could be made by introducing a Ag deficiency, which could then act as a way to control the carrier concentration. The LAST materials are thermally stable up to their melting point (> 1200 K), and doping is generally controlled by non-stoichiometry of the Ag, Pb, or Sb fractions in the form of $Ag_{1-x}Pb_{m+y}Sb_{1+z}Te_{2+m}$. The LAST-*m* ($m \approx 18$–22) system

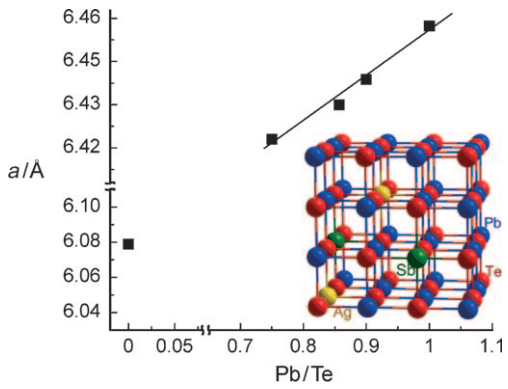

Figure 20. Lattice parameter values showing the LAST-*m* family follows Vegard's law, even though the system shows nanoscale phase segregation. In the NaCl-type lattice the cation sites are occupied by Ag, Sb, and Pb and the anion sites are occupied by Te.

showed a high power factor and rather low lattice thermal conductivity giving $ZT \approx 1.7$ at approximately 700 K.[201]

The LAST-*m* system is an interesting bulk-grown material that spontaneously forms nanostructures during cooling from the melt. High ZT values and nano-inclusions in the n-type $AgPb_mSbTe_{2+m}$ system were subsequently confirmed by additional reports.[202,203] Because of the complex nature of the phase diagram, the thermoelectric properties of these materials are extremely sensitive to the synthesis conditions.[204,205] As mentioned already in Section 3.2.2.2, even $AgSbTe_2$, one of the end members of the pseudobinary mixture, is prone to decompose into binary phases depending on synthetic conditions. It is necessary to keep these phenomena in mind when determining the appropriate synthesis.

Another approach to prepare the LAST-*m* composite is based on mechanical alloying and spark plasma sintering. Good thermoelectric performance was also obtained for LAST-*m* materials using this nanocomposite approach.[203] Polycrystalline $Ag_{0.8}Pb_{18+x}SbTe_{20}$ materials (very similar to LAST) formed by mechanical alloying of elemental powders followed by densification through spark plasma sintering achieved a ZT value of 1.5 at 673 K.[202] This is only 20% lower than the value reported by Hsu et al.[201,206] for the material grown from the melt. The average grain size of the nanocomposite was approximately 1 μm, with a compacted density of approximately 95% of the theoretical value. The observed approximately 20 nm-sized precipitates in the grains are believed to play an important role in lattice thermal-conductivity reduction, in similar way to the melt grown materials. The presence of Sb in these compositions is crucial to obtaining high ZT values as replacement with Bi results in lower power factors and higher lattice thermal conductivity (despite the presence of nanostructuring).[207] This result confirms that nanostructuring alone is not sufficient to reduce the thermal conductivity; it must enable enhanced phonon scattering (for example, through proper mass contrast or the presence of strain at the interface).

The highest power factor reported to date in this system, though relatively high, is still lower than that of optimized PbTe itself, indicating that electron scattering is somewhat increased. However, the lattice thermal conductivity is estimated to be only about 30% of that of PbTe and lower than what might be expected from a conventional solid-solution compound. Thus, the overall impact of the nano-inclusions in LAST-18 is a net enhancement of the ZT value compared to PbTe.

The nanoscale inclusions of minor phases in $AgPb_mSbTe_{2+m}$ exhibit coherent or semicoherent interfaces with the matrix. Cross-sectional transmission electron microscopy (TEM) shown in Figure 21 illustrates this relationship where coherence between the two regions is visible. This nanostructuring involves the endotaxial embedding of regions of one composition inside a matrix of another composition.[208]

The inclusions in the LAST-*m* materials are believed to form via thermodynamic spinodal decomposition or nucleation and growth events during cooling. These solid-state phenomena are nearly ideal mechanisms for the formation of phonon-scattering inclusions because, by its nature, the precipitate phase undergoes a series of coarsening steps

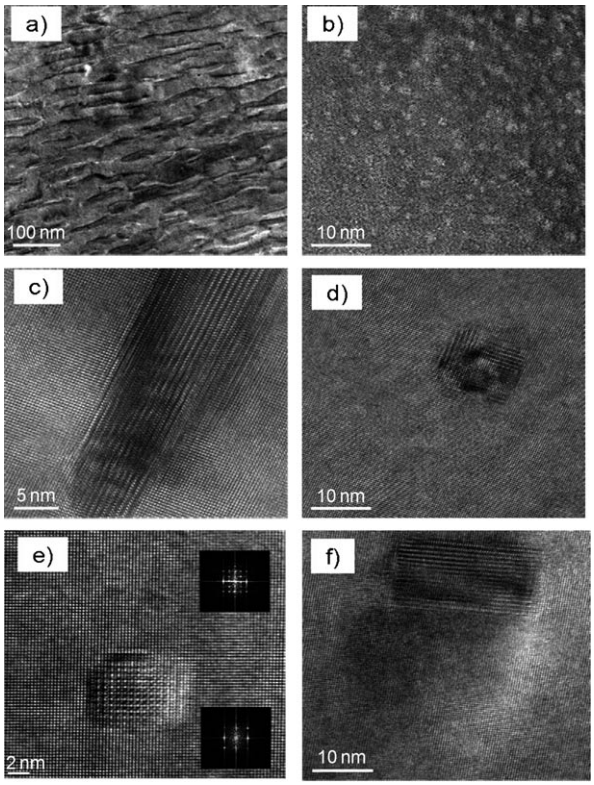

Figure 21. An assortment of images taken by HRTEM at various magnifications from LAST samples showing the complexity of the system on the atomic and nanoscale.

with coherent or semicoherent interfaces during the early stages.[209] Consequently, their composition, structure, as well as size and distribution can be controlled through judicious selection of cooling rate and post-synthesis heat treatment.

3.3.2. $AgPb_mSn_nSbTe_{2+m+n}$ (LASTT)

LASTT is a p-type analogue of the LAST-*m* family of materials based on the $Pb_{1-x}Sn_xTe$ solid solution.[210] ZT values for certain *m* and *n* values can reach 1.4 near 700 K. Presumably, the matrix in these nanocomposites is comprised of $Pb_{1-x}Sn_xTe$ solid solution and the nanoprecipitates are rich in Ag and Sb as was observed in LAST. However, in these materials the transport properties were not tuned as easily by varying the Ag or Sb concentrations as in the case of the Sn-free n-type material. However, the transport behavior in LASTT is more easily tuned through the Pb/Sn ratio with the 9/9 composition giving the optimum values of thermopower and electrical conductivity. Additional tuning, optimization, and scale up is currently underway and may give rise to a large-scale synthesis of high-ZT value p-type materials and devices.[211] In other compositions in the same family of compounds, novel properties emerge, such as in the case of $AgSnSbTe_3$, where a large Seebeck coefficient (160 $\mu V K^{-1}$) is measured even with nearly metallic carrier concentrations (ca. 5×10^{21} cm^{-3}).[212] Although other high-ZT value p-type materials have also been discovered and will be discussed in the following sections, LASTT may still be preferred as it is easy to prepare and does not contain thallium or sodium.

3.3.3. $NaPb_mSbTe_{2+m}$

The sodium-substituted system $NaPb_mSbTe_{2+m}$ (SALT-*m*: sodium antimony lead telluride) is also a high-performance system ($ZT\approx1.6$ at 675 K for $m\approx20$)[213] but has p-type behavior. Again, the impressive ZT value is attributed to the very low thermal conductivity of the material which is as low as 0.85 $W m^{-1} K^{-1}$, of which approximately 0.5 $W m^{-1} K^{-1}$ corresponds to the lattice contribution. In this case too, HRTEM images show a broad-based nano-segregated system with features similar to those exhibited by the LAST samples (Figure 22). The $NaPb_mSbTe_{m+2}$ system should be naturally

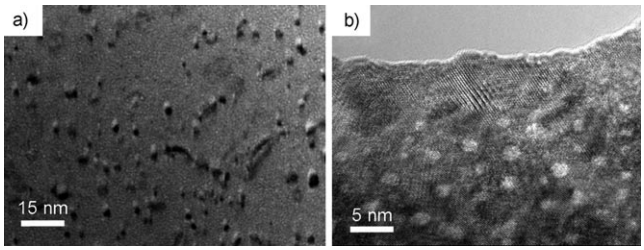

Figure 22. High-resolution TEM images of SALT-based composite materials clearly showing nanoscale precipitates.

prone to create Na-Sb-rich clusters in the lattice. The distribution of Na^+ and Sb^{3+} ions in the Pb^{2+} sublattice cannot be random as would be demanded by a solid solution, because coulombic forces alone tend to drive the system into clustering at the nanoscale thereby lowering the overall energy.[214] The ZT value of $Na_{0.95}Pb_{20}SbTe_{22}$ rises strongly with temperature and reaches 1 near 475 K and approximately 1.7 at 650 K. This is one of the widest temperature ranges in which a single material exhibits a ZT value above 1. Corresponding studies of $NaPb_mSn_nSbTe_{m+n+2}$ materials indicated that their thermoelectric performance did not exceed those of the SALT-*m* systems.[215]

3.3.4. PbTe-PbS

The discovery of nanodots in the LAST-*m* and SALT-*m* systems, coupled with the results observed for superlattice and endotaxially embedded nanocrystalline thin films, points to a new approach in thermoelectric materials exploration. This approach involves nanostructuring PbTe with a variety of inclusions. Spinodal decomposition occurs in the PbTe-PbS system where precipitates of PbS can be embedded in the PbTe matrix. Through investigation of the PbTe-PbS system for thermoelectric applications it was determined that the material actually has three scales of inhomogeneity simultaneously (Figure 23). The system $(PbTe)_{1-x}(PbS)_x$ does not form a solid solution, but rather phase separates into PbTe-rich and PbS-rich regions to produce coherent nanoscale heterogeneities.[216] For $x>0.03$, the materials are ordered on

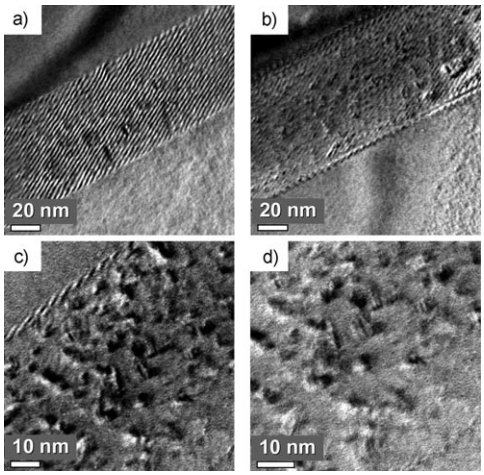

Figure 23. Transmission electron microscope images of PbTe-PbS (16%) showing various precipitates and compositional fluctuations formed in the sample through precipitation and growth and spinodal decomposition.

three submicron length scales. The coherent nanoinclusions in a close relative, $(Pb_{0.95}Sn_{0.05}Te)_{1-x}(PbS)_x$, do not lead to excessive electron scattering, and high electron mobilities of over $100\,cm^2V^{-1}s$ are observed at 700 K. At $x \approx 0.08$ the material achieves a very low room-temperature lattice thermal conductivity (ca. 30% that of PbTe), and $ZT \approx 1.5$ at 650 K is possible (Figure 24).[216]

An important question to ask is how much of the observed reduction in thermal conductivity in these systems is explicitly a result of the nanodots, because the systems typically have other co-existing defects—including solid–solution behavior—that are known to inhibit heat flow. Figure 25 shows the lattice thermal conductivities for five PbTe-based materials systems plus pure PbTe. It is clear that while solid–solution point-defect scattering alone is effective in lowering the κ_{latt} of PbTe by approximately 30–40%, nanostructuring contributes additional scattering to give an overall reduction of 75%.

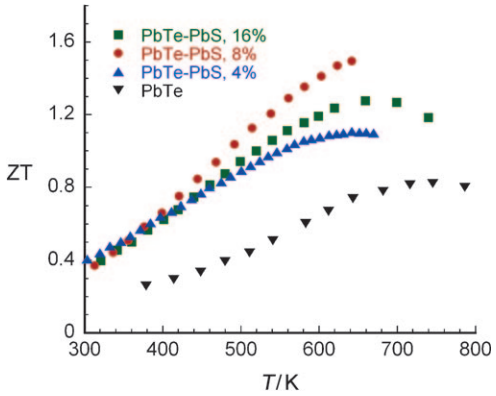

Figure 24. Measured ZT values for a series of PbTe-PbS composite materials doped with PbI_2 showing the improvements in ZT value that are possible by reducing the thermal conductivity through nanostructuring.

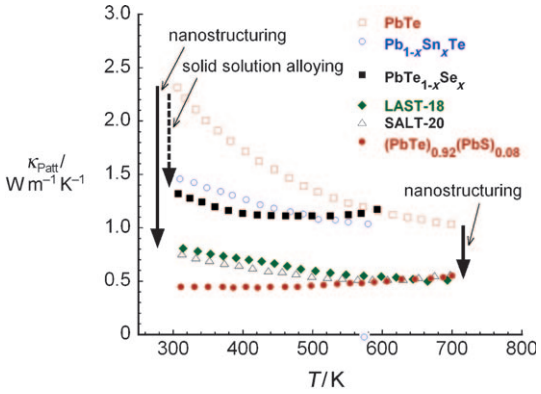

Figure 25. Lattice thermal conductivity as a function of temperature for various PbTe-based alloys and nanostructured samples.

3.3.5. *Nanostructured PbTe*

Precipitation and growth as well as matrix encapsulation can also be used to prepare nanocomposite materials based on a PbTe matrix. Similar reductions in lattice thermal conductivity to those found in the PbTe-PbS system have been observed in PbTe samples containing less than 3% of Sb nanoparticles (Figure 26a).[217] In contrast, similar fractions of

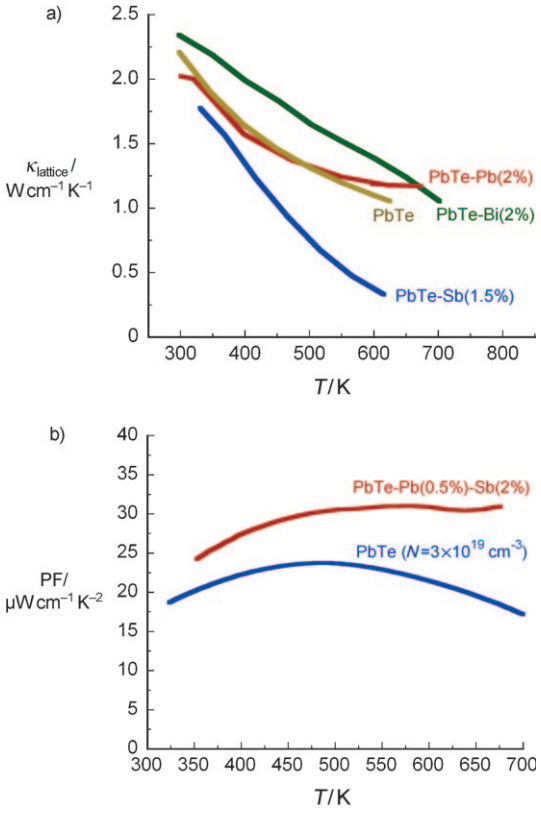

Figure 26. a) Lattice thermal conductivity of several PbTe based nanocomposite materials showing that Sb greatly reduces the thermal conductivity and Pb or Bi do not. b) Temperature-dependent power factor for PbTe nanostructured with Pb and Sb showing a clear enhancement (ca. 71%) over PbTe with the same carrier concentration.

nanoparticles of Bi or Pb (two elements that have the same atomic mass as the Pb ions in the rock salt lattice) were found to have no such effect.[217,218] It was however, determined that Pb nanoinclusions, not Sb, can be effective in increasing the Seebeck coefficient in PbTe albeit with concomitant reduction of the mobility and reduced ZT values.

Recently, PbTe co-nanostructured with both Pb and Sb precipitates has shown novel temperature-dependent behavior of the electron mobility and enhancements at high temperature result in an increase in ZT value to 1.4 at 673 K.[27] This nanostructured material may also present a method for increasing the power factor of thermoelectric materials as both an increased power factor and reduced thermal conductivity were observed in one material. For a given carrier concentration it is clear that the increased electrical conductivity at high temperatures is responsible for the increased power factor (Figure 26b). This increased electrical conductivity is a result of higher than expected mobility at high temperatures. The temperature dependence of the mobility in PbTe typically follows a power law ($\mu \approx T^{-2.5}$); however, in PbTe nanostructured with Pb and Sb the temperature dependence can be tuned by the Pb/Sb ratio. This change leads to larger mobilities at high temperature because the mobility decreases more slowly than in PbTe itself. This behavior was not observed in PbTe with Pb or Sb precipitates alone. Instead it can be inferred that a synergy between the two precipitates may be the cause of this unique behavior. Additionally, for the PbTe-Pb(0.5%)-Sb(2%) composition a substantial decrease in the lattice thermal conductivity was also observed. The exact mechanism and further understanding in this composite may shed light on mechanisms that could be applied generally to other thermoelectrics as well.

3.3.6. InGaAs:ErAs

This material system is in fact a thin-film system, but is covered herein because its lattice thermal conductivity behavior is very similar to the PbTe systems and reinforces the conclusion that nanoinclusions in a matrix can profoundly affect thermal transport in three-dimensional systems. The size distribution of ErAs nanoparticles in the matrix of InGaAs is not strongly linked to the growth parameters and the nanoparticles are typically 2–4 nm in diameter.[219] The volume fraction of the embedded nanoparticles can be easily changed from 0.01–6% without introducing defects or dislocations. Thermal-conductivity measurements show a reduction by as much as a factor of 3 compared to the bulk alloy. Detailed calculation of the phonon transport in ErAs:InGaAs for various nanoparticle sizes and distributions has shown that the significant reduction in lattice thermal conductivity is due to the scattering of mid- and long-wavelength phonons by the nanoparticles. These phonons are not effectively scattered by the point defects in a bulk alloy, which are more effective at scattering short-wavelength phonons. Calculations show that a wide size distribution of nanoparticles can effectively scatter different phonon modes and reduce thermal conductivity.

3.4. Nanocomposite Polycrystalline Materials

Recent approaches to achieve nanostructuring have been through the formation of polycrystalline nanosized samples (grain size ca. 5 nm–10 μm). Typically these are created by hot pressing or spark plasma sintering of fine powders that are formed by grinding and milling or wet-chemistry processing. The nanosized particles of the thermoelectric material are then hot pressed into monoliths. Instead of the nanoparticles-in-a-matrix model described above, this approach creates extensive interfacing between the compacted nanoparticles which can lower the thermal conductivity. The resulting sample can exhibit certain benefits over samples prepared by techniques that create very large-grain or single crystal material. These advantages include reduced thermal conductivity (through phonon scattering at grain boundaries), increased power factor (through to electron filtering at grain boundaries), better mechanical properties, and improved isotropy. Compacting nanocrystalline samples can be a relatively low-cost method to provide the large volume of material necessary for a more wide-spread use thermoelectric technology.[220] However, a major challenge with this approach is obtaining complete removal of any binder or organics used in the grinding, milling, or wet-chemistry processes, and obtaining as close to 100% of theoretical density during compaction as possible. If this is not successful, the carrier mobility will be substantially reduced (one order of magnitude or greater reduction for just a few percent decrease in density),[221] resulting in a lower ZT value. In addition to the examples described in detail below, this technique has been applied to several different classes of materials including PbTe[222–225] and skutterudite materials.[226–228]

Some promising results have recently been reported. An approach involving n-type nano/polycrystalline Bi_2Te_3 material resulted in a higher ZT value of 1.25 at 420 K compared to that of bulk Bi_2Te_3.[8] This material was prepared by hot pressing of a mix of nanometer-sized n-type Bi_2Te_3 and micron-sized powders together. The improvement in ZT value was attributed to a slight increase in electrical conductivity and a reduction (ca. 25%) in thermal conductivity. Additionally, Poudel et al.[220] obtained a ZT value of 1.2 at room temperature and 1.4 at 373 K from a ball-milled and hot-pressed p-type BiSbTe alloy. These values are about 20 and 40% higher, respectively, than the comparable state-of-the-art ingot BiSbTe alloy results they reported, with even greater improvement observed at higher temperatures. Interestingly, the observed electrical conductivity for the nanostructured material was also higher than the ingot material, an effect similar to that previously reported for the nanograined n-type material. The Seebeck coefficient was higher or lower depending on the temperature, yielding a slightly enhanced power factor for the nanostructured material. (It should be noted that it is unclear whether the carrier concentration was identical in the nanostructured and ingot materials.) The big improvement in the ZT value was attributed to a strongly reduced thermal conductivity and slightly increased power factor for the nanostructured material compared to the ingot, particularly at elevated temperatures. Using this nanostruc-

tured p-type material and a commercial n-type leg an approximately 20 K greater cooling capacity was reported compared to using commercial material for both the p- and n-legs. Nanocomposite boron-doped Si/Ge materials formed by ball milling and hot pressing were reported[221] to exhibit increased Seebeck coefficients and only slightly reduced electrical conductivities compared to bulk SiGe alloys (JIMO), resulting in a higher power factor for the nanocomposite material over the temperature range of 300–1000 K. The increased power factor for the nanocomposite is consistent with what was observed for the BiSbTe alloy, and as predicted based on electron-filtering effects at the grain boundaries. In addition, the thermal conductivity of the Si/Ge nanocomposite was significantly reduced over the entire temperature range, resulting in a peak ZT value of approximately 0.72 at 1000 K compared to a value of approximately 0.6 for the bulk SiGe alloy.

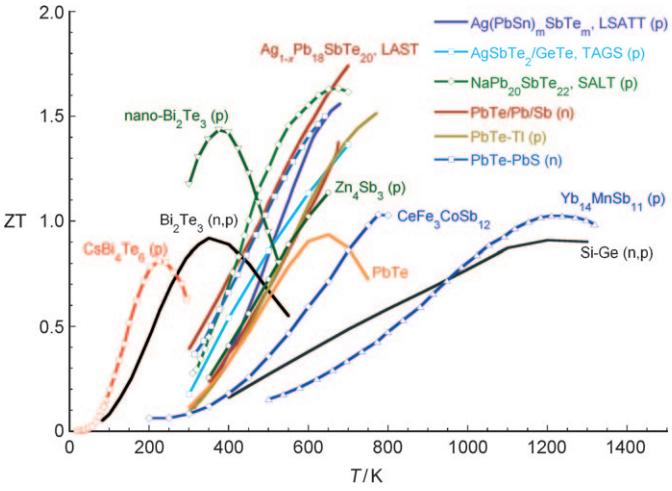

Figure 27. Plot of state-of-the-art thermoelectric materials highlighting recent advancements increasing ZT above 1.

4. Conclusions and Outlook

For over four decades the established approach to thermoelectric materials research has been to study crystalline single-phase materials with narrow band gaps, heavy elements, loaded with point defects created by the preparation of solid solutions (e.g. $Bi_{2-x}Sb_xTe_3$). The solid solutions are the key to achieve low thermal conductivity. In the current decade the discovery of stable nanostructures in LAST-*m* and related materials and the achievement of lower thermal conductivity than is possible with solid solutions alone has changed how we think about this research field. While studying new compounds to discover high ZT value materials is still a viable and attractive method, the nanostructured multiphase systems offer very promising, and more rational ways in this pursuit. In this context they define a new approach.

A common theme among many emerging thermoelectric materials is the concept of nanostructuring to improve the thermoelectric performance. In these systems the enhanced thermoelectric performance is attributable to a strong decrease in lattice thermal conductivity, rather than an increase in the electrical power factor. Thus, in certain cases nanodots clearly play a very significant role in reducing lattice thermal conductivity, probably by effectively scattering phonons that otherwise would have relatively long mean free paths. In many of these cases it has been clearly demonstrated that the reduction in thermal conductivity far exceeds any concomitant reduction in the power factor caused by electronic carrier scattering, thus resulting in enhanced ZT values. The ZT values of the current state of the art thermoelectric materials are shown in Figure 27.

Nanostructuring of thermoelectric materials for enhanced ZT values is thus gaining popularity, and it is a general approach that is broadly applicable to other bulk materials as well.[221,229] For example, recent reports on skutterudites[230] and half-Heusler alloys seem to confirm that real enhancements in ZT value by a thermal conductivity reduction are possible by introducing nanoinclusions.

Other mechanisms, guided by theoretical prediction, hold promise if they could be coupled with the reductions in thermal conductivity mentioned above. On example is the PbTe:Tl system where resonance states can be used to increase the Seebeck coefficient. Even further, changes in carrier mobility brought about by complex nanostructures, as in the co-nanostructured PbTe-Pb-Sb system, could also be applied to numerous other systems provided a better a theoretical understanding can be formulated.

The development of new materials and complex composites over the last 5–10 years has greatly increased the ZT values. It was through greater theoretical understanding, new synthesis techniques, and state-of-the-art measurements that the field has progressed so far and promises to advance further. For a long time it was thought that there was a practical barrier at ZT = 1, however new mechanisms for increasing both the power factor and reducing the thermal conductivity in thermoelectric materials continue to emerge and increase the ZT value. Today, the latest generation of bulk materials have ZT ≈ 1.6–1.7 at approximately 700–800 K. We hope that this new record will be broken and ZT ≈ 3 will soon be achieved. Future efforts in understanding and manipulating these mechanisms promise to increase the ZT value further and enable more practical application. It is apparent that the discovery of advanced thermoelectrics is a challenge well suitable for synthetic chemists to undertake. It is with innovative synthesis and creative thinking in materials design that new candidates will be identified and chemists are well trained in such endeavors. Therefore, we believe there are golden opportunities for synthesis in this field. Chemistry alone however is not enough to produce robust materials and functional thermoelectric modules and this requires close collaboration and reaching across scientific disciplines to ensure progress in the field.

Further reductions in the thermal conductivity alone may be sufficient to raise ZT values to 2, however to reach values of 3 or greater we also need dramatic enhancements in the power factor. Unless this is achieved with a welcome discovery of some new and unexpected single-phase material,

what is needed are new physical concepts on how the power factor can be enhanced 2–4-fold in the existing leading materials. In fact, such enhancements must come mainly from increases in the thermopower as opposed to increases in the electrical conductivity. How to do this is not currently clear and this is an open challenge to theorists and experimentalists alike to dream up new concepts that point to dramatic increases in the power factor.

We wish to add a note of caution. In several cases over optimism has hyped the potential of thermoelectrics for very large-scale energy-conversion applications and unnecessarily raised expectations beyond a point that is justified even by the prospects for achieving really high ZT values. The reality is more likely to be that even with significant increases in ZT ($\approx$1.6 or higher) the applications will not be in very large-scale power generation because even then they will not be competitive with steam turbines (i.e. MW or GW scale). Because steam turbines do not scale down well, it is realistic to expect that applications will be unique (i.e. those not served by other technologies) or will be limited to "distributed" modest-scale power production (several tens or hundreds of kW at a time).[1] This does not mean, however, that such applications will not be exciting or revolutionary. Nevertheless, despite the challenges mentioned above, in our opinion, the scientific and technological importance of thermoelectrics in meeting appropriate energy needs is evident and the prospects for it look promising.

The authors would like to thank the Office of Naval Research for financial support (grants N00014-02-1-0867, N00014-03-1-0789, N00014-06-1-0130, N00014-08-1-613). We express our deep appreciation to our collaborators including Professors T. Hogan, E. Case, H. Schock, S. D. Mahanti, C. Uher, K. M. Paraskevopoulos, T. Kyratsi, many students and postdocs in our group who have worked on the thermoelectric project and their names appear many references in this review. The authors also thank the US Department of Energy, Office of Basic Energy Sciences, under Contract No. DE-AC02-06CH11357.

Received: February 2, 2009

[1] C. B. Vining, *Nat. Mater.* **2009**, *8*, 83.
[2] D. Y. Chung, L. Iordanidis, K. S. Choi, M. G. Kanatzidis, *Bull. Korean Chem. Soc.* **1998**, *19*, 1283.
[3] F. J. DiSalvo, *Science* **1999**, *285*, 703.
[4] G. D. Mahan in *Solid State Physics*, *Vol. 51* (Ed.: F. S. H. Ehrenreich), Academic Press, New York, **1998**, p. 81.
[5] G. S. Nolas, J. Poon, M. Kanatzidis, *Mater. Res. Soc. Bull.* **2006**, *31*, 199.
[6] D. M. Rowe, *CRC Handbook of Thermoelectrics*, CRC, Boca Raton, FL, **1995**.
[7] D. M. Rowe, *Renewable Energy* **1999**, *16*, 1251.
[8] D. M. Rowe, *Thermoelectrics Handbook: Macro to Nano*, CRC/Taylor & Francis, Boca Raton, FL, **2006**.
[9] B. C. Sales, *Mater. Res. Soc. Bull.* **1998**, *23*, 15.
[10] T. M. Tritt, M. A. Subramanian, *Mater. Res. Soc. Bull.* **2006**, *31*, 188.
[11] C. Wood, *Rep. Prog. Phys.* **1988**, *51*, 459.
[12] H. Böttner, G. Chen, R. Venkatasubramanian, *MRS Bull.* **2006**, *31*, 211.
[13] G. Chen, *Semicond. Semimetals* **2001**, *71*, 203.
[14] G. Chen, M. S. Dresselhaus, J.-P. Fleurial, T. Caillat, *Int. Mater. Rev.* **2003**, *48*, 45.
[15] M. S. Dresselhaus, Y. M. Lin, S. B. Cronin, O. Rabin, M. R. Black, G. Dresselhaus, T. Koga, *Semicond. Semimetals* **2001**, *71*, 1.
[16] G. S. Kumar, G. Prasad, R. O. Pohl, *J. Mater. Sci.* **1993**, *28*, 4261.
[17] C. Kittel, *Introduction to Solid State Physics*, 8. Aufl., Wiley, New York, **2005**.
[18] R. W. Keyes, *Phys. Rev.* **1959**, *115*, 564.
[19] G. A. Slack, *CRC Handbook of Thermoelectrics* (Ed.: D. M. Rowe), CRC, Boca Raton, FL, **1995**, p. 407.
[20] B. C. Sales, B. C. Chakoumakos, D. Mandrus, J. W. Sharp, *J. Solid State Chem.* **1999**, *146*, 528.
[21] J. Donga, O. F. Sankey, G. K. Ramachandran, P. F. McMillan, *J. Appl. Phys.* **2000**, *87*, 7726.
[22] C. M. Bhandari, D. M. Rowe, *J. Phys. C* **1978**, *11*, 1787.
[23] J. W. Sharp, H. J. Goldsmid, in *Proc. 18th Int. Conf. Thermoelectrics* **1999**, p. 709.
[24] M. Masashi, F. Ryoji, *J. Solid State Chem.* **2005**, *178*, 1670.
[25] J. M. Zide, D. O. Klenov, S. Stemmer, A. C. Gossard, G. Zeng, J. E. Bowers, D. Vashaee, A. Shakouri, *Appl. Phys. Lett.* **2005**, *87*, 112102.
[26] D. Vashaee, A. Shakouri, *Phys. Rev. Lett.* **2004**, *92*, 106103.
[27] J. R. Sootsman, H. Kong, C. Uher, J. J. D'Angelo, C.-I. Wu, T. P. Hogan, T. Caillat, M. G. Kanatzidis, *Angew. Chem.* **2008**, *120*, 8746–8750; *Angew. Chem. Int. Ed.* **2008**, *47*, 8618.
[28] S. Iwanaga, M. Marciniak, R. B. Darling, F. S. Ohuchi, *J. Appl. Phys.* **2007**, *101*, 123709.
[29] G. M. Beensh-Marchwicka, E. Proclow, W. Mielcarek, *Cryst. Res. Technol.* **2001**, *36*, 1035.
[30] M. Ohtaki, D. Ogura, K. Eguchi, H. Arai, *J. Mater. Chem.* **1994**, *4*, 653.
[31] N. F. Mott, H. Jones, *The Theory of the Properties of Metals and Alloys*, Dover Publications, New York, **1958**.
[32] The carrier scattering between extrema needs to be minimum or zero.
[33] L. D. Hicks, M. S. Dresselhaus, *Phys. Rev. B* **1993**, *47*, 12727.
[34] P. Larson, S. D. Mahanti, M. G. Kanatzidis, *Phys. Rev. B* **2000**, *61*, 8162.
[35] G. Mahan, B. Sales, J. Sharp, *Phys. Today* **1997**, *50*, 42.
[36] L. E. Bell, *Science* **2008**, *321*, 1457.
[37] M. G. Kanatzidis, *Semicond. Semimetals* **2000**, *69*, 51.
[38] B. C. Sales, *Science* **2002**, *295*, 1248.
[39] G. J. Snyder, E. S. Toberer, *Nat. Mater.* **2008**, *7*, 105.
[40] W. Jeitschko, D. Braun, *Acta Crystallogr. Sect. B* **1977**, *33*, 3401.
[41] D. J. Braun, W. Jeitschko, *J. Less-Common Met.* **1980**, *72*, 147.
[42] D. J. Braun, W. Jeitschko, *J. Solid State Chem.* **1980**, *32*, 357.
[43] D. J. Braun, W. Jeitschko, *J. Less-Common Met.* **1980**, *76*, 33.
[44] B. C. Sales, D. Mandrus, B. C. Chakoumakos, V. Keppens, J. R. Thompson, *Phys. Rev. B* **1997**, *56*, 15081.
[45] G. S. Nolas, D. T. Morelli, T. M. Tritt, *Annu. Rev. Mater. Sci.* **1999**, *29*, 89.
[46] B. C. Sales in *Handbook on the Physics and Chemistry of the Rare Earths*, *Vol. 33* (Ed.: K. A. Gschneidner), Elsevier, New York, **2003**, p. 1.
[47] C. Uher, *Semicond. Semimetals* **2000**, *69*, 139.
[48] B. C. Sales, D. Mandrus, R. K. Williams, *Science* **1996**, *272*, 1325.
[49] G. S. Nolas, M. Kaeser, R. T. Littleton, T. M. Tritt, *Appl. Phys. Lett.* **2000**, *77*, 1855.
[50] X. Tang, L. Chen, T. Goto, T. Hirai, *J. Mater. Res.* **2001**, *16*, 837.
[51] D. T. Morelli, G. P. Meisner, B. Chen, S. Hu, C. Uher, *Phys. Rev. B* **1997**, *56*, 7376.
[52] L. D. Chen, T. Kawahara, X. F. Tang, T. Goto, T. Hirai, J. S. Dyck, W. Chen, C. Uher, *J. Appl. Phys.* **2001**, *90*, 1864.
[53] X. Tanga, Q. Zhang, L. Chen, T. Goto, T. Hirai, *J. Appl. Phys.* **2005**, *97*, 093712.

[54] M. Puyet, A. Dauscher, B. Lenoir, M. Dehmas, C. Stiewe, E. Müller, J. Hejtmanek, *J. Appl. Phys.* **2005**, *97*, 083712.
[55] J. S. Dyck, W. Chen, C. Uher, L. Chen, X. Tang, T. Hirai, *J. Appl. Phys.* **2002**, *91*, 3698.
[56] M. Puyet, B. Lenoir, A. Dauscher, M. Dehmas, C. Stiewe, E. Müller, *J. Appl. Phys.* **2004**, *95*, 4852.
[57] G. A. Slack, V. G. Tsoukala, *J. Appl. Phys.* **1994**, *76*, 1665.
[58] G. S. Nolas, G. A. Slack, S. B. Schujman in *Semiconductors and Semimetals*, *Vol. 69* (Ed.: T. M. Tritt), Academic Press, San Diego, **2001**, p. 255.
[59] G. S. Nolas, M. Beekman, J. Gryko, G. A. Lamberton, Jr., T. M. Tritt, P. F. McMillan, *Appl. Phys. Lett.* **2003**, *82*, 910.
[60] M. Beekman, G. S. Nolas, *J. Mater. Chem.* **2008**, *18*, 842.
[61] N. P. Blake, S. Latturner, J. D. Bryan, G. D. Stucky, H. Metiu, *J. Chem. Phys.* **2001**, *115*, 8060.
[62] G. S. Nolas, J. L. Cohn, G. A. Slack, S. B. Schujman, *Appl. Phys. Lett.* **1998**, *73*, 178.
[63] V. L. Kuznetsov, L. A. Kuznetsova, A. E. Kaliazin, D. M. Rowe, *J. Appl. Phys.* **2000**, *87*, 7871.
[64] A. Saramat, G. Svensson, A. E. C. Palmqvist, C. Stiewe, E. Mueller, D. Platzek, S. G. K. Williams, D. M. Rowe, J. D. Bryan, G. D. Stucky, *J. Appl. Phys.* **2006**, *99*, 023708.
[65] M. Christensen, G. J. Snyder, B. B. Iversen in *Proc. 25th Inter. Conf. Themoelectrics*, **2006**, p. 40.
[66] J.-H. Kim, N. L. Okamoto, K. Kishida, K. Tanaka, H. Inui, *Acta Mater.* **2006**, *54*, 2057.
[67] A. Bentien, V. Pacheco, S. Paschen, Y. Grin, F. Steglich, *Phys. Rev. B* **2005**, *71*, 165206.
[68] A. Bentien, M. Christensen, J. D. Bryan, A. Sanchez, S. Paschen, F. Steglich, G. D. Stucky, B. B. Iversen, *Phys. Rev. B* **2004**, *69*, 045107.
[69] G. K. H. Madsen, K. Schwarz, P. Blaha, D. J. Singh, *Phys. Rev. B* **2003**, *68*, 125212.
[70] W. Jeitschko, *Metall. Trans. A* **1970**, *1*, 3159.
[71] S. J. Poon, *Semicond. Semimetals* **2001**, *70*, 37.
[72] S. Ogut, K. M. Rabe, *Phys. Rev. B* **1995**, *51*, 10443.
[73] F. G. Aliev, N. B. Brandt, V. V. Moschalkov, V. V. Kozyrkov, R. V. Scolozdra, A. I. Belogorokhov, *Z. Phys. B* **1989**, *75*, 167.
[74] J. Tobola, J. Pierre, S. Kaprzyk, R. V. Skolozdra, M. A. Kouacou, *J. Phys. Condens. Matter* **1998**, *10*, 1013.
[75] C. Uher, J. Yang, S. Hu, D. T. Morelli, G. P. Meisner, *Phys. Rev. B* **1999**, *59*, 8615.
[76] Y. Xia, S. Bhattacharya, V. Ponnambalam, A. L. Pope, S. J. Poon, T. M. Tritt, *J. Appl. Phys.* **2000**, *88*, 1952.
[77] S. Bhattacharya, A. L. Pope, R. T. Littleton IV, T. M. Tritt, V. Ponnambalam, Y. Xia, S. J. Poon, *Appl. Phys. Lett.* **2000**, *77*, 2476.
[78] H. Hohl, A. P. Ramirez, C. Goldmann, G. Ernst, B. Wolfing, E. Bucher, *J. Phys. Condens. Matter* **1999**, *11*, 1697.
[79] S. Sportouch, P. Larson, M. Bastea, P. Brazis, J. Ireland, C. R. Kannewurf, S. D. Mahanti, C. Uher, M. G. Kanatzidis in *Mater. Res. Soc. Symp. Proc.*, *Vol. 545* (Eds.: T. M. Tritt, M. G. Kanatzidis, G. D. Mahan, H. B. Lyon, Jr.), Mater. Res. Soc., **1999**, p. 421.
[80] S. Sakurada, N. Shutoh, *Appl. Phys. Lett.* **2005**, *86*, 082105.
[81] Q. Shen, L. Chen, T. Goto, T. Hirai, J. Yang, G. P. Meisner, C. Uher, *Appl. Phys. Lett.* **2001**, *79*, 4165.
[82] J. Yang, H. Li, T. Wu, W. Zhang, L. Chen, J. Yang, *Adv. Funct. Mater.* **2008**, *18*, 2880.
[83] J. Yang, G. P. Meisner, L. Chen, *Appl. Phys. Lett.* **2004**, *85*, 1140.
[84] S. R. Culp, S. J. Poon, N. Hickman, T. M. Tritt, J. Blumm, *Appl. Phys. Lett.* **2006**, *88*, 042106.
[85] P. Larson, S. D. Mahanti, S. Sportouch, M. G. Kanatzidis, *Phys. Rev. B* **1999**, *59*, 15660.
[86] H. W. Mayer, I. Mikhail, K. Schubert, *J. Less-Common Met.* **1978**, *59*, 43.
[87] G. J. Snyder, M. Christensen, E. Nishibori, T. Caillat, B. B. Iversen, *Nat. Mater.* **2004**, *3*, 458.
[88] F. Cargnoni, E. Nishibori, P. Rabiller, L. Bertini, G. J. Snyder, M. Christensen, C. Gatti, B. B. Iversen, *Chem. Eur. J.* **2004**, *10*, 3861.
[89] T. Caillat, J.-P. Fleurial, A. Borshchevsky, *J. Phys. Chem. Solids* **1997**, *58*, 1119.
[90] M. Tsutsui, L. T. Zhang, K. Ito, M. Yamaguchi, *Intermetallics* **2004**, *12*, 809.
[91] V. L. Kuznetsov, D. M. Rowe, *J. Alloys Compd.* **2004**, *372*, 103.
[92] S. M. Kauzlarich, A. C. Payne, D. J. Webb in *Magnetism: Molecules to Materials III* (Eds.: J. S. Miler, M. Drillon), Wiley-VCH, Weinham, **2002**, p. 37.
[93] S. R. Brown, S. M. Kauzlarich, F. Gascoin, G. J. Snyder, *Chem. Mater.* **2006**, *18*, 1873.
[94] C. Wood, *Energy Convers. Manage.* **1984**, *24*, 331.
[95] O. Yamashita, N. Sadatomi, *J. Appl. Phys.* **2000**, *88*, 245.
[96] I. R. Fisher, S. L. Bud'ko, C. Song, P. C. Canfield, T. C. Ozawa, S. M. Kauzlarich, *Phys. Rev. Lett.* **2000**, *85*, 1120.
[97] S. M. Kauzlarich, S. R. Brown, G. J. Snyder, *Dalton Trans.* **2007**, 2099.
[98] A. Akrap, N. Barišić, L. Forro, D. Mandrus, B. C. Sales, *Phys. Rev. B* **2007**, *76*, 085203.
[99] I. Terasaki, Y. Sasago, K. Uchinokura, *Phys. Rev. B* **1997**, *56*, R12685.
[100] W. Koshibae, K. Tsutsui, S. Maekawa, *Phys. Rev. B* **2000**, *62*, 6869.
[101] Y. Wang, N. S. Rogado, R. J. Cava, N. P. Ong, *Nature* **2003**, *423*, 425.
[102] M. Ohtaki, Y. Nojiri, E. Maed, *Proc. 19th Int. Conf. Thermoelectrics*, IEEE, Wales, **2000**, p. 190.
[103] I. Terasaki, *Proc. 21st Int. Conf. Thermoelectrics*, **2002**, p. 185.
[104] K. Fujita, T. Mochida, K. Nakamura, *Jpn. J. Appl. Phys.* **2001**, *40*, 4644.
[105] A. Satake, H. Tanaka, T. Ohkawa, T. Fujii, I. Terasaki, *J. Appl. Phys.* **2004**, *96*, 931.
[106] M. Shikano, R. Funahashi, *Appl. Phys. Lett.* **2003**, *82*, 1851.
[107] R. Funahashi, I. Matsuhara, H. Ikuta, T. Takeuchi, U. Mizutani, S. Sodeoka, *Jpn. J. Appl. Phys.* **2000**, *39*, L1127.
[108] T. Yamamoto, K. Uchinokura, I. Tsukada, *Phys. Rev. B* **2002**, *65*, 184434.
[109] R. Funahashi, I. Matsuhara, *Appl. Phys. Lett.* **2001**, *79*, 362.
[110] T. Itoh, I. Terasaki, *Jpn. J. Appl. Phys.* **2000**, *39*, 6658.
[111] S. Hébert, S. Lambert, D. Pelloquin, A. Maignan, *Phys. Rev. B* **2001**, *64*, 172101.
[112] D. Pelloquin, A. Maignan, S. Hébert, C. Martin, M. Hervieu, C. Michel, L. B. Wang, B. Raveau, *Chem. Mater.* **2002**, *14*, 3100.
[113] I. Terasaki, *Proc. 24th Int. Conf. Thermoelectrics*, **2005**, p. 289.
[114] K. Koumoto, I. Terasaki, R. Funahashi, *Mater. Res. Soc. Bull.* **2006**, *31*, 206.
[115] M. Ohtaki, K. Tsubota, K. Eguchi, H. Arai, *J. Appl. Phys.* **1996**, *79*, 1816.
[116] T. Tsubota, M. Ohtaki, K. Eguchi, H. Arai, *J. Mater. Chem.* **1997**, *7*, 85.
[117] M. Ohtaki, S. Maehara, S. Shige, *Proc. 22th Int. Conf. Thermoelectrics*, **2003**, p. 171.
[118] H. Kaga, R. Asahi, T. Tani, *Jpn. J. Appl. Phys.* **2004**, *43*, 7133.
[119] R. Funahashi, S. Urata, *Int. J. Appl. Ceram. Technol.* **2007**, *4*, 297.
[120] A. Bentien, S. Johnsen, G. K. H. Madsen, B. B. Iversen, F. Steglich, *EPL* **2007**, *80*, 17008.
[121] A. Bentien, G. K. H. Madsen, S. Johnsen, B. B. Iversen, *Phys. Rev. B* **2006**, *74*, 205105.
[122] D. A. Wright, *Nat. Mater.* **1958**, *181*, 834.
[123] E. Skrabeck, D. S. Trimmer, *CRC Handbook of Thermoelectrics* (Ed.: D. M. Rowe), CRC, Boca Raton, FL, **1995**, p. 267.

[124] M. W. Oh, D. M. Wee, S. D. Park, B. S. Kim, H. W. Lee, *Phys. Rev. B* **2008**, *77*, 165119.
[125] B. Wölfing, C. Kloc, J. Teubner, E. Bucher, *Phys. Rev. Lett.* **2001**, *86*, 4350.
[126] J. W. Sharp, B. C. Sales, D. G. Mandrus, *Appl. Phys. Lett.* **1999**, *74*, 3794.
[127] D. Paccard, L. Paccard, G. Brun, J. C. Tedenac, *J. Alloys Compd.* **1992**, *184*, 337.
[128] K. Kurosaki, A. Kosuga, H. Muta, M. Uno, S. Yamanaka, *Appl. Phys. Lett.* **2005**, *87*, 061919.
[129] E. M. Godzhaev, R. A. Kerimova, *Inorg. Mater.* **2004**, *40*, 1153.
[130] T. J. McCarthy, T. A. Tanzer, M. G. Kanatzidis, *J. Am. Chem. Soc.* **1995**, *117*, 1294.
[131] M. G. Kanatzidis, T. J. McCarthy, T. A. Tanzer, L.-H. Chen, L. Iordanidis, T. Hogan, C. R. Kannewurf, C. Uher, B. Chen, *Chem. Mater.* **1996**, *8*, 1465.
[132] B. X. Chen, C. Uher, L. Iordanidis, M. G. Kanatzidis, *Chem. Mater.* **1997**, *9*, 1655.
[133] M. G. Kanatzidis, T. J. McCarthy, T. A. Tanzer, L.-H. Chen, T. Hogan, C. R. Kannewurf, L. Iordanidis, *Mater. Res. Soc. Symp. Proc.* **1996**, *410*, 37.
[134] D.-Y. Chung, T. Hogan, J. Schindler, L. Iordanidis, P. Brazis, C. R. Kannewurf, B. Chen, C. Uher, M. G. Kanatzidis, *Mater. Res. Soc. Symp. Proc.* **1997**, *478*, 333.
[135] T. J. Mccarthy, S. P. Ngeyi, J. H. Liao, D. C. Degroot, T. Hogan, C. R. Kannewurf, M. G. Kanatzidis, *Chem. Mater.* **1993**, *5*, 331.
[136] D. Y. Chung, K. S. Choi, L. Iordanidis, J. L. Schindler, P. W. Brazis, C. R. Kannewurf, B. X. Chen, S. Q. Hu, C. Uher, M. G. Kanatzidis, *Chem. Mater.* **1997**, *9*, 3060.
[137] L. Iordanidis, M. G. Kanatzidis, *Angew. Chem.* **2000**, *112*, 2003; *Angew. Chem. Int. Ed.* **2000**, *39*, 1927.
[138] D. Y. Chung, S. Jobic, T. Hogan, C. R. Kannewurf, R. Brec, J. Rouxel, M. G. Kanatzidis, *J. Am. Chem. Soc.* **1997**, *119*, 2505.
[139] D. Y. Chung, T. Hogan, P. Brazis, M. Rocci-Lane, C. Kannewurf, M. Bastea, C. Uher, M. G. Kanatzidis, *Science* **2000**, *287*, 1024.
[140] L. Iordanidis, J. L. Schindler, C. R. Kannewurf, M. G. Kanatzidis, *J. Solid State Chem.* **1999**, *143*, 151.
[141] K. S. Choi, L. Iordanidis, K. Chondroudis, M. G. Kanatzidis, *Inorg. Chem.* **1997**, *36*, 3804.
[142] D. Y. Chung, L. Iordanidis, K. K. Rangan, P. W. Brazis, C. R. Kannewurf, M. G. Kanatzidis, *Chem. Mater.* **1999**, *11*, 1352.
[143] A. Mrotzek, D. Y. Chung, T. Hogan, M. G. Kanatzidis, *J. Mater. Chem.* **2000**, *10*, 1667.
[144] K. S. Choi, D. Y. Chung, A. Mrotzek, P. Brazis, C. R. Kannewurf, C. Uher, W. Chen, T. Hogan, M. G. Kanatzidis, *Chem. Mater.* **2001**, *13*, 756.
[145] K. Adouby, C. Perez Vicente, J. C. Jumas, R. Fourcade, A. Abba Touré, *Z. Kristallogr.* **1998**, *213*, 343.
[146] C. Pérez Vicente, J. L. Tirado, K. Adouby, J. C. Jumas, A. Abba Touré, G. Kra, *Inorg. Chem.* **1999**, *38*, 2131.
[147] W. Choe, S. Lee, P. O'Connell, A. Covey, *Chem. Mater.* **1997**, *9*, 2025.
[148] Y. C. Wang, F. J. DiSalvo, *Chem. Mater.* **2000**, *12*, 1011.
[149] L. Iordanidis, P. W. Brazis, C. R. Kannewurf, M. G. Kanatzidis, *Mater. Res. Soc. Symp. Proc.* **1999**, *545*, 189.
[150] M. G. Kanatzidis, D.-Y. Chung, L. Iordanidis, K.-S. Choi, P. W. Brazis, T. Hogan, C. R. Kannewurf, *Mater. Res. Soc. Symp. Proc.* **1999**, *545*, 233.
[151] G. A. Slack in *Solid State Physics*, *Vol. 34* (Ed.: H. S. F. Ehrenreich, D. Turnbull), Academic Press, New York, **1997**, p. 1.
[152] P. W. Brazis, J. R. Ireland, M. A. Lane, T. M. Kyratsi, D.-Y. Chung, M. G. Kanatzidis, C. R. Kannewurf, *Mater. Res. Soc. Symp. Proc.* **2000**, *626*, Z8.11.
[153] T. Kyratsi, J. S. Dyck, W. Chen, D. Y. Chung, C. Uher, K. M. Paraskevopoulos, M. G. Kanatzidis, *J. Appl. Phys.* **2002**, *92*, 965.
[154] T. Kyratsi, E. Hatzikraniotis, K. M. Paraskevopoulos, C. D. Malliakas, J. S. Dyck, C. Uher, M. G. Kanatzidis, *J. Appl. Phys.* **2006**, *100*, 123704.
[155] T. Kyratsi, E. Hatzikraniotis, M. Paraskevopoulous, J. S. Dyck, H. K. Shin, C. Uher, M. G. Kanatzidis, *J. Appl. Phys.* **2004**, *95*, 4140.
[156] T. Kyratsi, D. Y. Chung, M. G. Kanatzidis, *J. Alloys Compd.* **2002**, *338*, 36.
[157] T. Kyratsi, D. Y. Chung, J. R. Ireland, C. R. Kannewurf, M. G. Kanatzidis, *Chem. Mater.* **2003**, *15*, 3035.
[158] T. Kyratsi, M. G. Kanatzidis, *Z. Anorg. Allg. Chem.* **2003**, *629*, 2222.
[159] J. F. Meng, N. V. C. Shekar, D. Y. Chung, M. Kanatzidis, J. V. Badding, *J. Appl. Phys.* **2003**, *94*, 4485.
[160] D. I. Bilc, S. D. Mahanti, T. Kyratsi, D.-Y. Chung, M. G. Kanatzidis, P. Larson, *Phys. Rev. B* **2005**, *71*, 085116.
[161] D. Y. Chung, T. P. Hogan, M. Rocci-Lane, P. Brazis, J. R. Ireland, C. R. Kannewurf, M. Bastea, C. Uher, M. G. Kanatzidis, *J. Am. Chem. Soc.* **2004**, *126*, 6414.
[162] V. A. Greanya, W. C. Tonjes, R. Liu, C. G. Olson, D.-Y. Chung, M. G. Kanatzidis, *Phys. Rev. B* **2002**, *65*, 205123.
[163] L. Lykke, B. B. Iversen, G. K. H. Madsen, *Phys. Rev. B* **2006**, *73*, 195121.
[164] P. Larson, S. D. Mahanti, D. Y. Chung, M. G. Kanatzidis, *Phys. Rev. B* **2002**, *65*.
[165] R. Venkatasubramanian, E. Siivola, T. Colpitts, B. O'Quinn, *Nature* **2001**, *413*, 597.
[166] X. B. Zhao, X. H. Ji, Y. H. Zhang, T. J. Zhu, J. P. Tu, X. B. Zhang, *Appl. Phys. Lett.* **2005**, *86*, 062111.
[167] X. B. Xiao, T. J. Zhu, X. H. Ji in *Thermoelectrics Handbook: Macro to Nano* (Ed.: D. M. Rowe), CRC, Boca Raton, FL, **2006**, p. 25.
[168] X. Tang, W. Xie, H. Li, W. Zhao, Q. Zhang, *Appl. Phys. Lett.* **2007**, *90*, 012102.
[169] B. Poudel, Q. Hao, Y. Ma, Y. Lan, A. Minnich, B. Yu, X. Yan, D. Wang, A. Muto, D. Vashaee, X. Chen, J. Liu, M. S. Dresselhaus, G. Chen, Z. Ren, *Science* **2008**, *320*, 634.
[170] Z. H. Dughaish, *Phys. B* **2002**, *322*, 205.
[171] Yu. I. Ravich, B. A. Efimova, I. A. Smirnov, *Semiconducting Lead Chalcogenides*, *Vol. 5*, Plenum, New York, **1970**.
[172] F. Ren, E. D. Case, J. R. Sootsman, M. G. Kanatzidis, H. Kong, C. Uher, E. Lara-Curzio, R. M. Trejo, *Acta Mater.* **2008**, *56*, 5954.
[173] Y. Gelbstein, Z. Dashevsky, M. P. Dariel, *J. Appl. Phys.* **2008**, *104*, 033702.
[174] Y. Gelbstein, G. Gotesman, Y. Lishzinker, Z. Dashevsky, M. P. Dariel, *Scr. Mater.* **2007**, *58*, 251.
[175] K. Hoang, S. D. Mahanti, *Phys. Rev. B* **2008**, *78*, 085111.
[176] S. D. Mahanti, K. Hoang, S. Ahmad, *Phys. B* **2007**, *401–402*, 291.
[177] K. Hoang, S. D. Mahanti, P. Jena, *Phys. Rev. B* **2007**, *76*, 115432.
[178] S. Ahmad, S. D. Mahanti, K. Hoang, M. G. Kanatzidis, *Phys. Rev. B* **2006**, *74*, 155205.
[179] V. Jovovic, S. J. Thiagarajan, J. P. Heremans, T. Komissarova, D. Khokhlov, A. Nicorici, *J. Appl. Phys.* **2008**, *103*, 053710.
[180] J. P. Heremans, V. Jovovic, E. S. Toberer, A. Saramat, K. Kurosaki, A. Charoenphakdee, S. Yamanaka, G. J. Snyder, *Science* **2008**, *321*, 554.
[181] P. F. P. Poudeu, J. D'Angelo, A. Downey, R. Pcionek, J. Sootsman, Z. Zhou, O. Palchik, T. P. Hogan, C. Uher, M. G. Kanatzidis, *Mater. Res. Soc. Symp. Proc.* **2006**, *886*, 195.
[182] P. F. P. Poudeu, J. D'Angelo, H. Kong, A. Downey, J. L. Short, R. Pcionek, T. P. Hogan, C. Uher, M. G. Kanatzidis, *J. Am. Chem. Soc.* **2006**, *128*, 14347.
[183] G. Offergeld, J. M. Gilles, H. Hatwell, J. Vancakenberghe, *C. R. Hebd. Seances Acad. Sci.* **1961**, *252*, 3788.
[184] S. Geller, J. H. Wernick, *Acta Crystallogr.* **1959**, *12*, 46.

[185] J. H. Wernick, S. Geller, K. E. Benson, *J. Phys. Chem. Solid* **1958**, *7*, 240.
[186] S. S. Ragimov, S. A. Aliev, *Inorg. Mater.* **2007**, *43*, 1184.
[187] T. Ishihara, *J. Phys. Soc. Jpn.* **1962**, *17*, 719.
[188] T. Irie, *J. Phys. Soc. Jpn.* **1962**, *17*, 1810.
[189] R. Wolfe, J. H. Wernick, S. E. Haszko, *J. Appl. Phys.* **1960**, *31*, 1959.
[190] K. Hoang, S. D. Mahanti, J. R. Salvador, M. G. Kanatzidis, *Phys. Rev. Lett.* **2007**, *99*, 156403.
[191] L. H. Ye, K. Hoang, A. J. Freeman, S. D. Mahanti, J. He, T. M. Tritt, M. G. Kanatzidis, *Phys. Rev. B* **2008**, *77*, 245203.
[192] D. T. Morelli, V. Jovovic, J. P. Heremans, *Phys. Rev. Lett.* **2008**, *101*, 035901.
[193] V. Jovovic, J. P. Heremans, *Phys. Rev. B* **2008**, *77*, 245204.
[194] S. K. Plachkova, *Phys. Status Solidi A* **1984**, *83*, 349.
[195] E. Skrabek, D. Trimmer, U.S. Patent no. 3945855, **1976**.
[196] F. D. Rosi, J. P. Dismukes, E. F. Hockings, *Electr. Eng.* **1960**, *79*, 450.
[197] B. A. Cook, M. J. Kramer, X. Wei, J. L. Harringa, E. M. Levin, *J. Appl. Phys.* **2007**, *101*, 053715.
[198] B. A. Cook, X. Wei, J. L. Harringa, M. J. Kramer, *J. Mater. Sci.* **2007**, *42*, 7643.
[199] S. H. Yang, T. J. Zhu, T. Sun, S. N. Zhang, X. B. Zhao, J. He, *Nanotechnology* **2008**, *19*, 245707.
[200] G. C. Christakudis, S. K. Plachkova, L. E. Shelimova, E. S. Avilov, *Phys. Status Solidi A* **1991**, *128*, 465.
[201] K. F. Hsu, S. Loo, F. Guo, W. Chen, J. S. Dyck, C. Uher, T. Hogan, E. K. Polychroniadis, M. G. Kanatzidis, *Science* **2004**, *303*, 818.
[202] M. Zhou, J.-F. Li, T. Kita, *J. Am. Chem. Soc.* **2008**, *130*, 4527.
[203] H. Wang, J. F. Li, C. W. Nan, M. Zhou, W. S. Liu, B. P. Zhang, T. Kita, *Appl. Phys. Lett.* **2006**, *88*, 092104.
[204] T. J. Zhu, F. Yan, S. N. Zhang, X. B. Zhao, *J. Phys. D* **2007**, *40*, 3537.
[205] H. S. Dow, M. W. Oh, S. D. Park, B. S. Kim, B. K. Min, H. W. Lee, D. M. Wee, *J. Appl. Phys.* **2009**, *105*, 113703.
[206] M.-K. Han, K. Hoang, H. Kong, R. Pcionek, C. Uher, K. M. Paraskevopoulos, S. D. Mahanti, M. G. Kanatzidis, *Chem. Mater.* **2008**, *20*, 3512.
[207] E. Quarez, K. F. Hsu, R. Pcionek, N. Frangis, E. K. Polychroniadis, M. G. Kanatzidis, *J. Am. Chem. Soc.* **2005**, *127*, 9177.
[208] J. D. Verhoeven, *Fundamentals of Physical Metallurgy*, Wiley, New York, **1975**.
[209] J. Androulakis, K. F. Hsu, R. Pcionek, H. Kong, C. Uher, J. J. D'Angelo, A. Downey, T. Hogan, M. G. Kanatzidis, *Adv. Mater.* **2006**, *18*, 1170.
[210] T. P. Hogan, A. Downey, J. Short, J. D'Angelo, C.-I. Wu, E. Quarez, J. Androulakis, P. F. P. Poudeu, J. R. Sootsman, D.-Y. Chung, M. G. Kanatzidis, S. D. Mahanti, E. J. Timm, H. Schock, F. Ren, J. Johnson, E. D. Case, *J. Electron. Mater.* **2007**, *36*, 704.
[211] J. Androulakis, R. Pcionek, E. Quarez, J.-H. Do, H. Kong, O. Palchik, C. Uher, J. J. D'Angelo, J. Short, T. Hogan, M. G. Kanatzidis, *Chem. Mater.* **2006**, *18*, 4719.
[212] P. F. P. Poudeu, J. D'Angelo, A. D. Downey, J. L. Short, T. P. Hogan, M. G. Kanatzidis, *Angew. Chem.* **2006**, *118*, 3919; *Angew. Chem. Int. Ed.* **2006**, *45*, 3835.
[213] K. Hoang, K. Desai, S. D. Mahanti, *Phys. Rev. B* **2005**, *72*, 064102.
[214] A. Gueguen, P. F. P. Poudeu, C.-P. Li, S. Moses, C. Uher, J. He, V. Dravid, K. M. Paraskevopoulos, M. G. Kanatzidis, *Chem. Mater.* **2009**, *21*, 1683.
[215] J. Androulakis, C. H. Lin, H. J. Kong, C. Uher, C. I. Wu, T. Hogan, B. A. Cook, T. Caillat, K. M. Paraskevopoulos, M. G. Kanatzidis, *J. Am. Chem. Soc.* **2007**, *129*, 9780.
[216] J. R. Sootsman, R. J. Pcionek, H. Kong, C. Uher, M. G. Kanatzidis, *Chem. Mater.* **2006**, *18*, 4993.
[217] J. P. Heremans, C. M. Thrush, D. T. Morelli, *Phys. Rev. B* **2004**, *70*, 115334.
[218] W. Kim, J. Zide, A. Gossard, D. Klenov, S. Stemmer, A. Shakouri, A. Majumdar, *Phys. Rev. Lett.* **2006**, *96*, 045901.
[219] B. Poudel, Q. Hao, Y. Ma, Y. Lan, A. Minnich, B. Yu, X. Yan, D. Wang, A. Muto, D. Vashaee, X. Chen, J. Liu, M. S. Dresselhaus, G. Chen, Z. Ren, *Science* **2008**, *320*, 634.
[220] M. S. Dresselhaus, G. Chen, M. Y. Tang, R. G. Yang, H. Lee, D. Z. Wang, Z. F. Ren, J. P. Fleurial, P. Gogna, *Adv. Mater.* **2007**, *19*, 1043.
[221] J. Martin, S. Stefanoski, L. Wang, L. Chen, G. S. Nolas, *Mater. Res. Soc. Symp. Proc.* **2008**, *1044*.
[222] J. Martin, G. S. Nolas, W. Zhang, L. Chen, *Appl. Phys. Lett.* **2007**, *90*, 222112.
[223] X. Ji, B. Zhang, T. M. Tritt, J. W. Kolis, A. Kumbhar, *J. Electron. Mater.* **2007**, *36*, 721.
[224] T. M. Tritt, B. Zhang, N. Gothard, J. He, X. Ji, D. Thompson, J. W. Kolis, *Mater. Res. Soc. Symp. Proc.* **2006**, *886*, 53.
[225] X. Ji, J. He, P. N. Alboni, T. M. Tritt, J. W. Kolis, *Mater. Res. Soc. Symp. Proc.* **2008**, *1044*.
[226] P. N. Alboni, X. Ji, J. He, N. Gothard, T. M. Tritt, *J. Appl. Phys.* **2008**, *103*, 113707.
[227] X. Ji, J. He, P. Alboni, Z. Su, N. Gothard, B. Zhang, T. M. Tritt, J. W. Kolis, *Phys. Status Solidi RRL* **2007**, *1*, 229.
[228] W. X. Tian, R. G. Yang, *Appl. Phys. Lett.* **2007**, *90*, 263105.
[229] J. L. Mi, X. B. Zhao, T. J. Zhu, J. P. Tu, *Appl. Phys. Lett.* **2007**, *91*, 172116.
[230] H. Li, X. F. Tang, X. L. Su, Q. J. Zhang, C. Uher, *J. Phys. D Appl. Phys.* **2009**, *42*, 145409.